Libertas Academica
FREEDOM TO RESEARCH

Open Access: Full open access to this and thousands of other papers at http://www.la-press.com.

Gene Regulation and Systems Biology

A Comprehensive Profile of ChIP-Seq-Based PU.1/Spi1 Target Genes in Microglia

Jun-ichi Satoh, Naohiro Asahina, Shouta Kitano and Yoshihiro Kino

Department of Bioinformatics and Molecular Neuropathology, Meiji Pharmaceutical University, Kiyose, Tokyo, Japan.

ABSTRACT: Microglia are resident mononuclear phagocytes that play a principal role in the maintenance of normal tissue homeostasis in the central nervous system (CNS). Microglia, rapidly activated in response to proinflammatory stimuli, are accumulated in brain lesions of neurodegenerative diseases, such as Alzheimer's disease and Parkinson's disease. The E26 transformation-specific (ETS) family transcription factor PU.1/Spi1 acts as a master regulator of myeloid and lymphoid development. PU.1-deficient mice show a complete loss of microglia, indicating that PU.1 plays a pivotal role in microgliogenesis. However, the comprehensive profile of PU.1/Spi1 target genes in microglia remains unknown. By analyzing a chromatin immunoprecipitation followed by deep sequencing (ChIP-Seq) dataset numbered SRP036026 with the Strand NGS program, we identified 5,264 Spi1 target protein-coding genes in BV2 mouse microglial cells. They included *Spi1*, *Irf8*, *Runx1*, *Csf1r*, *Csf1*, *Il34*, *Aif1* (*Iba1*), *Cx3cr1*, *Trem2*, and *Tyrobp*. By motif analysis, we found that the PU-box consensus sequences were accumulated in the genomic regions surrounding ChIP-Seq peaks. By using pathway analysis tools of bioinformatics, we found that ChIP-Seq-based Spi1 target genes show a significant relationship with diverse pathways essential for normal function of monocytes/macrophages, such as endocytosis, Fc receptor-mediated phagocytosis, and lysosomal degradation. These results suggest that PU.1/Spi1 plays a crucial role in regulation of the genes relevant to specialized functions of microglia. Therefore, aberrant regulation of PU.1 target genes might contribute to the development of neurodegenerative diseases with accumulation of activated microglia.

KEYWORDS: ChIP-Seq, GenomeJack, KeyMolnet, microglia, microgliopathy, Nasu–Hakola disease, PU.1, Spi1, Strand NGS

CITATION: Satoh et al. A Comprehensive Profile of ChIP-Seq-Based PU.1/Spi1 Target Genes in Microglia. *Gene Regulation and Systems Biology* 2014:8 127–139 doi: 10.4137/GRSB.S19711.

RECEIVED: September 1, 2014. **RESUBMITTED:** November 2, 2014. **ACCEPTED FOR PUBLICATION:** November 10, 2014.

ACADEMIC EDITOR: James Willey, Editor in Chief

TYPE: Original Research

FUNDING: This work was supported by the JSPS KAKENHI (C25430054), the Ministry of Education, Culture, Sports, Science and Technology (MEXT), Japan, and the grant from the National Center for Geriatrics and Gerontology (NCGC26–20). The authors confirmed that the funder had no influence over the study design, content of the article, or selection of this journal.

COMPETING INTERESTS: The authors declare no competing interests.

CORRESPONDENCE: satoj@my-pharm.ac.jp

Paper subject to independent expert blind peer review by minimum of two reviewers. All editorial decisions made by independent academic editor. Upon submission manuscript was subject to anti-plagiarism scanning. Prior to publication all authors have given signed confirmation of agreement to article publication and compliance with all applicable ethical and legal requirements, including the accuracy of author and contributor information, disclosure of competing interests and funding sources, compliance with ethical requirements relating to human and animal study participants, and compliance with any copyright requirements of third parties. This journal is a member of the Committee on Publication Ethics (COPE).

Introduction

Microglia are resident mononuclear phagocytes that play a principal role in the maintenance of normal tissue homeostasis in the central nervous system (CNS).[1] They are derived from primitive c-kit$^+$ erythromyeloid precursors (EMPs) in the yolk sac emerging as early as on day 8 post-conception during embryogenesis.[2,3] EMPs develop into CD45$^+$ c-kit^{lo} CX3CR1$^-$ immature A1 cells that subsequently differentiate into CD45$^+$ c-kit$^-$ CX3CR1$^+$ A2 cells. Proliferating A2 cells enter into the developing CNS and are incorporated into the brain parenchyma as resident microglia. Microglia have a capacity to constantly scavenge invading pathogens, dying cells, and unwanted synapses by sensing them with a panel of pattern recognition receptors (PRRs).[1] Microglia show a ramified morphology under physiological conditions. When exposed to infectious and traumatic stimuli, they rapidly adopt an amoeboid morphology, followed by secretion of various cytokines, chemokines, and reactive oxygen and nitrogen species. Depending on their microenvironment, microglia are activated to acquire two distinct priming states. Stimulation with lipopolysaccharide (LPS) or interferon-gamma (IFNγ) induces the "classically" activated (M1; proinflammatory) state relevant to defense against bacterial and viral infection, whereas exposure to interleukin (IL)-4 or IL-13 promotes the conversion to the "alternatively" activated (M2; anti-inflammatory) state involved in tissue repair and remodeling.[1]

Microglia play a central role in the pathophysiology of human neurodegenerative diseases that are characterized by chronic inflammation associated with accumulation of activated microglia in affected areas, such as Alzheimer's disease (AD), Parkinson's disease (PD), and Huntington's disease (HD).[4,5] In AD, amyloid-beta (Aβ) activates microglia by signaling through Toll-like receptors (TLRs) and NOD-like receptors (NLRs), leading to production of proinflammatory mediators potentially toxic to neurons.[6,7] In PD, alpha-synuclein (α-Syn), which serves as a danger-associated molecular pattern, directly activates microglia.[8] In HD, mutant huntingtin promotes transcriptional activation of numerous proinflammatory genes in microglia.[9] However, at present, the precise mechanism underlying gene regulation relevant to microglial activation in human neurodegenerative diseases remains largely unknown.

The E26 transformation-specific (ETS) family transcription factor PU.1, also named as Spi1 or Sfpi1 in mouse, acts as a master regulator of myeloid and lymphoid development, expressed chiefly in monocytes/macrophages, neutrophils, mast cells, B cells, and early erythroblasts.[10] PU.1 comprises an N-terminal transactivation domain, a C-terminal DNA-binding domain, and an intervening PEST domain for protein–protein interactions. It activates expression of hundreds of downstream genes by binding to a purine-rich DNA sequence named the PU-box located on the targets. The expression levels of PU.1 target genes are highly variable in different cell types, owing to the difference in cellular concentration of PU.1, chromatin accessibility, motif-binding affinity, and cooperation with neighboring transcription factors.[11] Importantly, PU.1-deficient mice show a complete loss of microglia, along with a lack of mature macrophages, monocytes, neutrophils, and B cells, indicating that PU.1 regulates key genes involved in differentiation and maturation of not only hematopoietic cells but also brain microglia.[12,13] However, at present, the comprehensive profile of PU.1 target genes involved in microgliogenesis remains uncharacterized. In the adult human microglia, MCSF (CSF1) treatment elevates the expression levels of PU.1 and stimulates phagocytosis of Aβ, while knockdown of PU.1 reduces their viability and phagocytic capability.[14,15] Interferon regulatory factor 8 (Irf8) serves as an essential regulator of development of A2 microglial progenitor cells.[3] Irf8-deficient microglia show fewer elaborated processes with decreased expression of Iba1 and reduced proliferative and phagocytic activities.[16] Runt-related transcription factor 1 (Runx1), whose expression levels are elevated in amoeboid microglia, promotes reverse transition from amoeboid to ramified microglia.[17]

Recently, the rapid progress in the next-generation sequencing (NGS) technology has revolutionized the field of genome research. Chromatin immunoprecipitation followed by deep sequencing (ChIP-Seq) serves as one of NGS applications for genome-wide profiling of DNA-binding proteins, histone modifications, and nucleosomes.[18] ChIP-Seq, with advantages of higher resolution, less noise, and greater coverage of the genome, compared with microarray-based ChIP-Chip, provides an innovative tool for studying gene regulatory networks on the whole genome scale. Furthermore, recent advances in systems biology help us to investigate the cell-wide map of the complex molecular interactions by using the literature-based knowledgebase of molecular pathways.[19] Therefore, the integration of high dimensional ChIP-Seq NGS data with underlying molecular networks represents a rational approach to characterize the genome-wide network-based molecular mechanisms of gene regulation. To clarify the biological role of PU.1 in regulation of microglial functions, we attempted to characterize the comprehensive set of ChIP-Seq-based PU.1/Spi1 target genes in microglial cells by analyzing a dataset retrieved from public database.

Methods

ChIP-Seq dataset of microglial cells. A ChIP-Seq dataset of microglial cells was retrieved from DDBJ Sequence Read Archive (DRA) under the accession number SRP036026. The researchers in Dr. Christopher K. Glass's Laboratory, University of California, San Diego, performed the original experiment to study the role of reactive microglia in HD.[9] The raw data are open to public from March 2, 2014. Currently, no alternative datasets are publicly available for PU.1 ChIP-Seq of microglia. They cloned the N-terminus of wild-type (15Q) or mutant (128Q) human huntingtin in the pCDH-CMV-MCS-EF1-Puro vector (System Bioscience). Either the cloned vector or the empty vector was expressed in BV2 mouse microglial cells,[20] by using the Lentiviral expression system (System Bioscience). Then, they were processed for ChIP-Seq analysis. We studied ChIP-Seq data derived from the cells transduced with the empty vector (no exogenous huntingtin). Following fixation with formaldehyde, sonicated nuclear lysates were immunoprecipitated with a rabbit polyclonal anti-PU.1 (Spi1) antibody (sc-352; Santa Cruz Biotechnology) (SRX451619) or a rabbit polyclonal anti-CCAAT-enhancer-binding protein alpha (C/EBPα, Cebpa) antibody (sc-61; Santa Cruz Biotechnology) (SRX451622). NGS libraries constructed from adapter-ligated ChIP DNA fragments were processed for deep sequencing on Genome Analyzer IIx (Illumina).

First, we evaluated the quality of NGS short reads by searching them on the FastQC program (www.bioinformatics.babraham.ac.uk/projects/fastqc). Then, we removed the reads of insufficient quality by filtering them out with the FASTX-toolkit (hannonlab.cshl.edu/fastx_toolkit). After cleaning the data, we mapped them on the mouse genome reference sequence version mm9 by a mapping tool named COBWeb of the Strand NGS2.0 program, formerly named Avadis NGS (Strand Genomics), or by the Bowtie2 version 2.1.0 program (bowtie-bio.sourceforge.net/bowtie2/index.shtml). Then, we identified the peaks of binding sites with fold enrichment (FE) ≥5 by using the Model-based Analysis of ChIP-Seq (MACS) program or the Probabilistic Inference for ChIP-Seq (PICS)

program.[21,22] We determined the genes corresponding to the peaks by a neighboring gene analysis tool of Strand NGS in the setting within a distance of 5,000 bp from peaks to genes. We characterized the genomic location of binding peaks by a peak-finding tool of Strand NGS that classifies the locations into the upstream region, 5' untranslated region (5'UTR), exon, intron, and 3'UTR. We also imported the processed data into a genome viewer named GenomeJack v1.4 (Mitsubishi Space Software). We identified the consensus motif sequences in the genomic regions surrounding the peaks by using the GADEM program.[23]

Molecular network analysis. To identify molecular networks biologically relevant to ChIP-Seq-based Spi1 target genes, we imported the corresponding Entrez Gene IDs into the Functional Annotation tool of Database for Annotation, Visualization and Integrated Discovery (DAVID) v6.7 (david.abcc.ncifcrf.gov).[24] DAVID identifies relevant pathways constructed by Kyoto Encyclopedia of Genes and Genomes (KEGG), composed of the genes enriched in the given set, followed by statistical evaluation by a modified Fisher's exact test corrected by Bonferroni multiple comparison test. KEGG (www.kegg.jp) is a publicly accessible knowledgebase that covers a wide range of pathway maps on metabolic, genetic, environmental, and cellular processes, and human diseases, currently composed of 332,680 pathways generated from 466 reference pathways.[25]

We also imported Entrez Gene IDs into Ingenuity Pathways Analysis (IPA) (Ingenuity Systems; www.ingenuity.com). IPA is a commercial knowledgebase that contains approximately 3,000,000 biological and chemical interactions and functional annotations with definite scientific evidence. Upon uploading the list of Gene IDs, the network-generation algorithm identifies focused genes integrated in global molecular pathways and networks. IPA calculates the score *P*-value that reflects the statistical significance of association between the genes and the pathways or networks by the Fisher's exact test.

KeyMolnet (KM Data; www.km-data.jp), a different commercial knowledgebase, contains manually curated content on 164,000 relationships among human genes and proteins, small molecules, diseases, pathways, and drugs.[26] They include the core content collected from selected review articles with the highest reliability. Upon importing the list of Gene IDs, KeyMolnet automatically provides corresponding molecules as nodes on the network. The neighboring network-search algorithm selected one or more molecules as starting points to generate the network of all kinds of molecular interactions around starting molecules, including direct activation/inactivation, transcriptional activation/repression, and the complex formation within one path from starting points. The generated network was compared side by side with 501 human canonical pathways of the KeyMolnet library. The algorithm counting the number of overlapping molecular relations between the extracted network and the canonical pathway makes it possible to identify the canonical pathway showing the most significant contribution to the extracted network.

Results

Identification of 5,264 ChIP-Seq-based Spi1 target genes in mouse microglia. First, we evaluated the quality of ChIP-Seq NGS data examined in the present study. After cleaning, the quality scores mostly exceeded 30 across the bases on FastQC, indicating an acceptable quality for downstream analysis (Supplementary Fig. 1, panels a, b). After mapping them on mm9 by COBWeb, we identified 56,278 Spi1-ChIP peaks detected by MACS and 15,141 Spi1-ChIP peaks detected by PICS. From these, we selected peaks located within a distance of 5,000 bp from protein coding genes, and then extracted 5,264 genes overlapping between data derived from two distinct peak-finding algorithms MACS and PICS termed as the most reliable Spi1 targets (Supplementary Table 1). The peaks were accumulated in the upstream (18.7%) and intronic (69.5%) regions. The motif analysis by GADEM revealed an existence of the PU-box consensus sequences defined as 5'-GAGGAA-3' located within the genomic regions surrounding ChIP-Seq peaks (Fig. 1).

We identified both *Spi1* (FE = 19.3) and *Irf8* (FE = 27.8) in the list of Spi1 target genes (Supplementary Table 1; Figs. 2 and 3). Both of them are known to serve as a crucial regulator of differentiation of microglia from EMPs during early embryogenesis.[3] We also found *Runx1* (FE = 26.7), a transcription factor acting to constitute a negative feedback loop of PU.1,[27] along with *Csf1r* (FE = 10.7), *Csf1* (FE = 17.8), and *Il34* (FE = 31.5), acting as a key growth factor for differentiation of microglia,[28] as Spi1 targets (Supplementary Table 1). Furthermore, we identified known cell type-specific markers for microglia, such as *Aif1* (Iba1, FE = 32.9), *Cx3cr1*

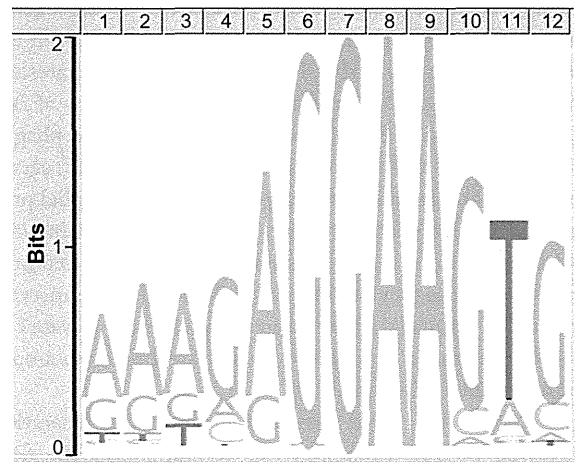

Figure 1. Spi1-binding consensus sequence motif. The consensus motif sequences surrounding Spi1 ChIP-Seq peaks were identified by the GADEM program. The PU-box consensus sequences defined as 5'-GAGGAA-3' were located on 80.3% of the peaks detected by MACS.

Figure 2. Genomic location of Spi1 ChIP-Seq peak on the *Spi1* gene. The genomic location of Spi1 ChIP-Seq peaks was determined by importing the processed data into GenomeJack. An example of transcription factor PU.1 (Spi1; Entrez Gene ID 20375) is shown, where a MACS peak numbered 66326 in the Spi1.bam Coverage track is located in the promoter region of the *Spi1* gene (panel a) with a Spi1-binding consensus sequence motif highlighted by orange square (panel b).

(FE = 17.8), *Cd68* (FE = 20.3), *Trem2* (FE = 12.8), and *Tyrobp* (Dap12) (FE = 14.6) in the list of Spi1 target genes (Supplementary Table 1; Supplementary Figs. 2 and 3). Importantly, loss of function of either TREM2 or DAP12, components of a receptor/adapter complex on human microglia, plays a causative role in Nasu–Hakola disease (NHD).[29] Furthermore, we found *Syk* (FE = 17.8), a downstream signal transducer of the Trem2/Dap12 pathway, as a Spi1 target gene.

Next, we studied ChIP-Seq-based Cebpa target genes in BV2 microglial cells. We identified 12,685 Cebpa-ChIP peaks detected by MACS and 10,311 Cebpa-ChIP peaks detected by PICS. From these, we selected peaks located within a distance of 5,000 bp from protein coding genes, and then extracted 3,106 genes overlapping between data derived from MACS and PICS termed as the most reliable Cebpa targets. We found that 1,844 genes are shared between Spi1 targets and Cebpa targets, suggesting the possibility that Cebpa coregulates a substantial proportion (35%) of Spi1 target genes in microglial cells (Supplementary Table 1, underline).

A recent study by direct RNA sequencing of flow cytometry-sorted mouse brain microglia has characterized a set of 100 transcripts exclusively expressed in microglia.[30] The study designated them as "the microglial sensome" (Supplementary Table 2). Importantly, we found that 63 out of 100 microglial sensome genes correspond to ChIP-Seq-based Spi1 target genes, indicating that Spi1 plays a pivotal role in regulation of the genes relevant to specialized functions of microglia (Table 1).

Molecular networks of ChIP-Seq-based Spi1 target genes in microglia. Next, we studied molecular networks of the set of 5,264 ChIP-Seq-based Spi1 target genes by using three distinct pathway analysis tools of bioinformatics. By using DAVID, we identified functionally associated gene ontology (GO) terms. The most significant GO terms included "phosphate metabolic process" (GO:0006796; P = 2.21E-16 corrected by Bonferroni multiple comparison test) for biological process, "plasma membrane" (GO:0005886; P = 1.26E-15) for cellular component, and "GTPase regulator activity" (GO:0030695; P = 1.27E-22) for molecular function.

By using KEGG, we found that the set of 5,264 Spi1 targets showed a significant relationship with the pathways defined as "Lysosome" (mmu04142; P = 5.08E-08 corrected by Bonferroni multiple comparison test), "Focal adhesion" (mmu04510; P = 1.27E-07), "Endocytosis" (mmu04144; P = 4.54E-07), "Fcγ receptor-mediated phagocytosis" (mmu04666; P = 5.03E-07) (Fig. 4), and "MAPK signaling pathway" (mmu04010; P = 6.23E-06) (Table 2). Furthermore, they also exhibited significant association with the pathways

Figure 3. Genomic location of Spi1 ChIP-Seq peak on the *Irf8* gene. The genomic location of Spi1 ChIP-Seq peaks was determined by importing the processed data into GenomeJack. An example of interferon regulatory factor 8 (Irf8; Entrez Gene ID 15900) is shown, where a MACS peak numbered 111561 in the Spi1.bam Coverage track is located in the intronic region of the *Irf8* gene (panel a) with a Spi1-binding consensus sequence motif highlighted by orange square (panel b).

defined as "Pathways in cancer" (mmu05200; P=1.39E-04), "B cell receptor signaling pathway" (mmu04662; P = 2.18E-04), "Apoptosis" (mmu04210; P = 4.23E-04), "Leukocyte transendothelial migration" (mmu04670; P= 6.57E-04), "Chemokine signaling pathway" (mmu04062; P= 8.52E-04), and "Chronic myeloid leukemia" (mmu05220; P = 1.16E-03) (Table 2). Importantly, the top-ranked "Lysosome" pathway included the set of 10 cathepsin genes, such as *Ctsa, Ctsb, Ctsc, Ctsd, Ctse, Ctsf, Ctsk, Ctsl, Ctss,* and *Ctsz*, essential for degradation of lysosomal proteins in microglia (Table 2).

Next, we studied molecular networks of 5,264 Spi1 target genes by using the core analysis tool of IPA. They showed a significant relationship with canonical pathways defined as "Fcγ receptor-mediated phagocytosis in macrophages and monocytes" (P=2.11E-15), "Molecular mechanisms of cancer" (P=6.92E-15), "B cell receptor signaling" (P=2.77E-14), "Role of NFAT in regulation of the immune response" (P=1.17E-12), and "PI3K signaling in B lymphocytes" (P = 2.15E-12). The results of KEGG and IPA combined together indicated that Spi1 regulates expression of not only the genes crucial for normal function of monocytes/macrophages and B cells but also those involved in oncogenesis, particularly in leukemogenesis. IPA also identified functional networks relevant to Spi1 target genes (Supplementary Table 3). The most significant network was defined as "Cell Morphology, Cellular Function and Maintenance, Cell Death and Survival" (P = 1.00E-53), where key components of autophagosomes, such as ATG3, ATG5, ATG7, and ATG10, are clustered (Fig. 5). The second rank network represented "RNA Post-Transcriptional Modification, Cellular Assembly and Organization, Infectious Disease" (P = 1.00E-53).

Finally, we studied molecular networks of 5,264 Spi1 target genes by using KeyMolnet. The neighboring network-search algorithm extracted the highly complex network composed of 5,788 molecules and 13,719 molecular relations (Supplementary Fig. 4). It showed the most significant relationship with "Transcriptional regulation by RB/E2F" (P = 7.27E-193). We identified *Rb1* (FE = 17.7), *Rbl1* (FE = 25.8), *Rbl2* (FE = 37.1), and *E2f1* (FE = 18.6) as a group of Spi1 target genes (Supplementary Table 1).

Discussion

Mice lacking PU.1/Spi1 are devoid of microglia, indicating that PU.1 acts as an indispensable transcription factor for development and differentiation of microglia.[13,31,32] By analyzing a ChIP-Seq dataset, we identified 5,264 Spi1 target protein-coding genes in BV2 mouse microglial cells. BV2 cells are derived from immortalized microglia of newborn

Table 1. The set of 63 microglial sensome genes corresponding to ChIP-Seq-based Spi1 target genes.

CHROMOSOME	START OF PEAKS	END OF PEAKS	FOLD ENRICHMENT	ENTREZ GENE ID	GENE SYMBOL	GENE NAME
chr7	132757191	132757492	38.659794	60504	Il21r	interleukin 21 receptor
chr3	89709374	89709685	37.668518	16194	Il6ra	interleukin 6 receptor, alpha
chr6	122902489	122902814	37.181004	73149	Clec4a3	C-type lectin domain family 4, member a3
chr11	60955751	60956142	35.720745	57916	Tnfrsf13b	tumor necrosis factor receptor superfamily, member 13b
chrX	13213539	13213888	33.61721	23890	Gpr34	G protein-coupled receptor 34
chr4	66504343	66504608	33.29038	21898	Tlr4	toll-like receptor 4
chr7	108112592	108113189	33.136967	233571	P2ry6	pyrimidinergic receptor P2Y, G-protein coupled, 6
chr18	35879188	35879366	32.216496	68545	Ecscr	endothelial cell-specific chemotaxis regulator
chr4	149501529	149501774	30.927835	56485	Slc2a5	solute carrier family 2 (facilitated glucose transporter), member 5
chr3	30763607	30763924	30.746971	71862	Gpr160	G protein-coupled receptor 160
chr7	16829398	16829780	29.842648	319430	C5ar2	complement component 5a receptor 2
chr11	120818969	120819371	29.78236	80879	Slc16a3	solute carrier family 16 (monocarboxylic acid transporters), member 3
chr1	121972010	121972524	28.747026	170706	Tmem37	transmembrane protein 37
chr9	110948641	110949068	27.061855	17002	Ltf	lactotransferrin
chr9	116075399	116075615	26.661926	21813	Tgfbr2	transforming growth factor, beta receptor II
chr18	60966814	60967338	26.09944	16149	Cd74	CD74 antigen (invariant polypeptide of major histocompatibility complex, class II antigen-associated)
chr5	114094521	114094878	26.044493	14747	Cmklr1	chemokine-like receptor 1
chr7	135258809	135259228	25.773195	16409	Itgam	integrin alpha M
chr13	37488117	37488288	25.773195	17084	Ly86	lymphocyte antigen 86
chr3	106592873	106593332	25.472342	12508	Cd53	CD53 antigen
chr16	38789019	38789447	25.28691	22268	Upk1b	uroplakin 1B
chr11	46280548	46280823	24.811836	171285	Havcr2	hepatitis A virus cellular receptor 2
chr6	40535749	40536059	24.257126	23845	Clec5a	C-type lectin domain family 5, member a
chr11	78799024	78799325	23.375689	16859	Lgals9	lectin, galactose binding, soluble 9
chr13	103496918	103497108	22.680412	17079	Cd180	CD180 antigen
chr3	105735367	105735926	22.315817	433638	I830077J02Rik	RIKEN cDNA I830077J02 gene
chr5	65352028	65352431	21.753523	21899	Tlr6	toll-like receptor 6
chr16	36642687	36643132	21.577559	12524	Cd86	CD86 antigen
chr1	140026784	140027054	21.477663	19264	Ptprc	protein tyrosine phosphatase, receptor type, C
chr7	106859678	106859981	21.273113	101488	Slco2b1	solute carrier organic anion transporter family, member 2b1
chr6	122805926	122806252	20.940722	12267	C3ar1	complement component 3a receptor 1
chr7	16849252	16849697	20.837904	12273	C5ar1	complement component 5a receptor 1

chr4	132139773	132139985	20.618557	19204	Ptafr	platelet-activating factor receptor
chr19	40782595	40783023	20.34726	12495	Entpd1	ectonucleoside triphosphate diphosphohydrolase 1
chr11	69479440	69480081	20.306154	12514	Cd68	CD68 antigen
chr1	172903138	172903598	20.071161	14130	Fcgr2b	Fc receptor, IgG, low affinity IIb
chr10	19317003	19317223	19.63672	15979	Ifngr1	interferon gamma receptor 1
chr3	87180536	87180918	19.435524	229499	Fcrl1	Fc receptor-like 1
chr6	125030472	125030733	19.091257	381810	Lpar5	lysophosphatidic acid receptor 5
chr3	59064135	59064423	19.032515	70839	P2ry12	purinergic receptor P2Y, G-protein coupled 12
chr16	33947248	33947454	18.990776	16419	Itgb5	integrin beta 5
chr1	172989424	172989659	18.93541	14131	Fcgr3	Fc receptor, IgG, low affinity III
chr4	133654539	133654895	18.744143	23833	Cd52	CD52 antigen
chr7	4018702	4019029	18.126204	52855	Lair1	leukocyte-associated Ig-like receptor 1
chrX	103346689	103346910	17.842981	279572	Tlr13	toll-like receptor 13
chr9	119977884	119978196	17.774618	13051	Cx3cr1	chemokine (C-X3-C) receptor 1
chr1	174408269	174408572	17.634293	98365	Slamf9	SLAM family member 9
chr3	100835299	100835620	16.568483	630146	Cd101	CD101 antigen
chr2	93289154	93289478	16.108248	12521	Cd82	CD82 antigen
chr4	47408473	47408654	16.108248	21812	Tgfbr1	transforming growth factor, beta receptor I
chr3	105716542	105717356	15.942183	11542	Adora3	adenosine A3 receptor
chr15	103140748	103141572	14.66406	80910	Gpr84	G protein-coupled receptor 84
chr7	31198532	31198988	14.567458	22177	Tyrobp	TYRO protein tyrosine kinase binding protein
chr5	138278454	138278742	14.318442	231805	Pilra	paired immunoglobin-like type 2 receptor alpha
chr3	96097068	96098277	14.087213	14129	Fcgr1	Fc receptor, IgG, high affinity I
chr9	114661993	114662369	14.058106	67213	Cmtm6	CKLF-like MARVEL transmembrane domain containing 6
chr17	48491514	48491850	12.772557	83433	Trem2	triggering receptor expressed on myeloid cells 2
chr15	78135354	78135537	12.326311	12984	Csf2rb2	colony stimulating factor 2 receptor, beta 2, low-affinity (granulocyte-macrophage)
chr18	61280165	61280583	10.698308	12978	Csf1r	colony stimulating factor 1 receptor
chr1	172948811	172949254	10.376222	246256	Fcgr4	Fc receptor, IgG, low affinity IV
chr4	144830530	144830848	9.163803	21938	Tnfrsf1b	tumor necrosis factor receptor superfamily, member 1b
chr10	59834857	59835131	8.8232565	74048	4632428N05Rik	RIKEN cDNA 4632428N05 gene
chr9	20820541	20820889	7.9916887	15894	Icam1	intercellular adhesion molecule 1

Notes: From the ChIP-Seq dataset, we identified 5,264 Spi1-target genes in BV2 mopuse microglia showing fold enrichment (FE) ≥5. Among them, those corresponding to microglial sensome genes (Supplementary Table 2) are listed with the chromosome, the position of the peak (start, end), FE, Entrez Gene ID, Gene Symbol, and Gene Name. The Cebpa-target genes are underlined.

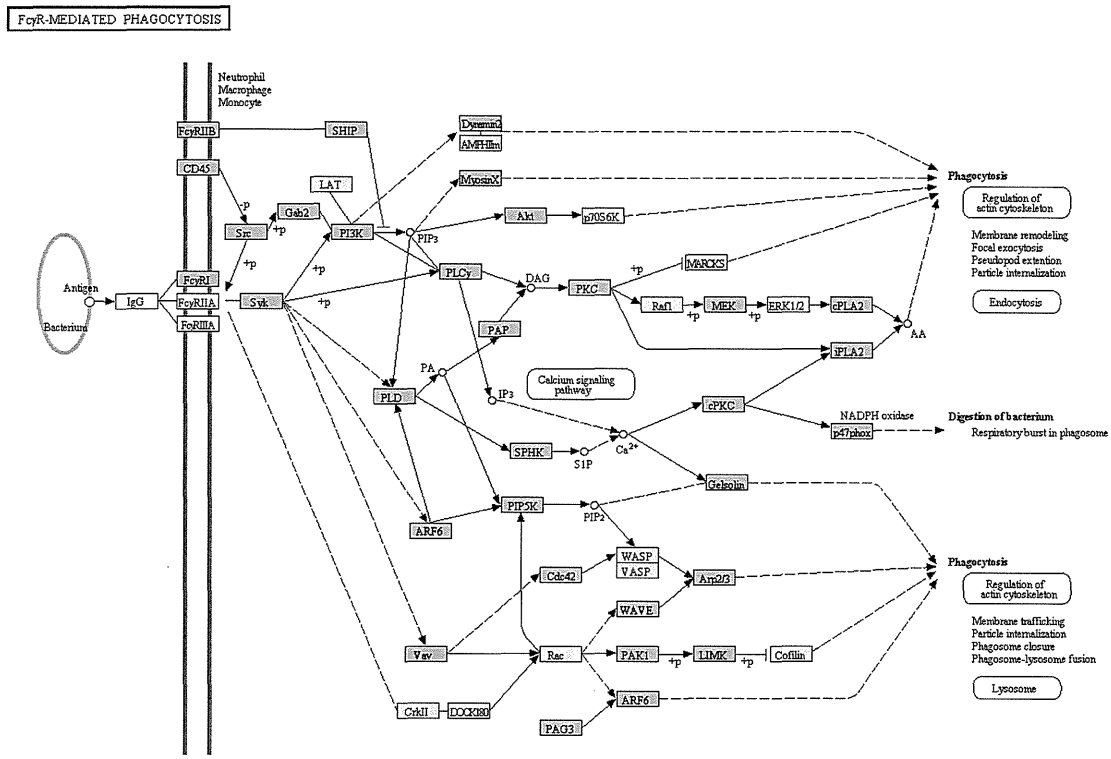

Figure 4. KEGG "Fcγ receptor-mediated phagocytosis" pathway relevant to Spi1 target genes. Entrez Gene IDs of 5,264 ChIP-Seq-based Spi1 target genes were imported into the Functional Annotation tool of DAVID. It extracted the KEGG "Fcγ receptor-mediated phagocytosis" pathway (mmu04666) as the fourth rank significant pathway as listed in Table 2. Spi1 target genes are colored by orange.

mouse origin that express morphological, phenotypical, and functional characteristics of primary microglia.[33] We extracted the genes overlapping between data derived from two distinct peak-finding algorithms MACS and PICS termed as the set of most reliable Spi1 targets. Enrichment of the PU-box consensus sequences within the genomic regions surrounding ChIP-Seq peaks validated the reliability of our analysis. By using pathway analysis tools named KEGG and IPA, we found that ChIP-Seq-based Spi1 target genes show a significant relationship with diverse pathways essential for normal function of monocytes/macrophages, such as endocytosis, Fcγ receptor-mediated phagocytosis, and lysosomal degradation, along with the pathway closely related to leukemogenesis. Relevantly, mice with reduced expression of PU.1 develop acute myeloid leukemia.[34] Approximately two-thirds (63%) of "microglial sensome" genes that reflect the microglia-specific gene signature[30] corresponded to Spi1 targets. These observations suggest that Spi1 plays a pivotal role in regulation of the genes relevant to specialized functions of microglia. KeyMolnet constructed the complex network of Spi1 target genes showing the most significant relationship with transcriptional regulation by RB/E2F. PU.1, capable of interacting physically with the C pocket of phosphorylated retinoblastoma (Rb) protein, blocks erythroid differentiation by repressing GATA-1 in mouse erythroleukemia cells.[35]

The set of 5,264 Spi1 target genes include Spi1 itself, supporting the previous observations that PU.1 activates its own promoter elements via an autoregulatory loop.[36] We found that approximately one-third of Spi1 target genes in microglia are potentially coregulated by Cebpa, a transcription factor essential for the development of monocytic and granulocytic lineage cells.[37] Importantly, Cebpa directly activates PU.1 gene transcription by binding to its promoter and distal enhancer.[38] A previous study showed that the Cebpa–Spi1 pathway plays a central role in regulation of microglial proliferation in a mouse model of prion diseases.[39]

NHD is a rare autosomal recessive disorder characterized by progressive dementia and multifocal bone cysts, caused by genetic mutations of either *DAP12* or *TREM2*.[29] Pathologically, NHD brains exhibit extensive demyelination and gliosis distributed predominantly in the frontal and temporal lobes and the basal ganglia, accompanied by marked accumulation of axonal spheroids and microglia.[40] TREM2 acts as a phagocytic receptor expressed on osteoclasts, dendritic cells, macrophages, and microglia, where it constitutes a signaling complex with an adaptor molecule DAP12, leading to phosphorylation and activation of the downstream kinase Syk. TREM2 expressed on microglia plays a key role in the clearance of damaged neural tissues to resolve damage-induced inflammation.[41] We identified *Trem2*, *Tyrobp* (*Dap12*), and

Table 2. KEGG pathways relevant to ChIP-Seq-based Spi1 target genes in microglia.

RANK	CATEGORY	FOCUSED GENES IN THE PATHWAY	*P*-VALUE CORRECTED BY BONFERRONI	FDR
1	mmu04142: Lysosome	Abcb9, Ap1b1, Ap1g1, Ap1s3, Ap3b1, Ap3b2, Ap3m2, Ap3s2, Ap4e1, Ap4s1, Arsa, Arsb, Arsg, Atp6v0a1, Atp6v0c, Atp6v0d1, Atp6v0d2, Cd68, Clta, Cltb, Cltc, Ctsa, Ctsb, Ctsc, Ctsd, Ctse, Ctsf, Ctsk, Ctsl, Ctss, Ctsz, Ctns, Fuca1, Galc, Gga1, Gla, Gnptab, Gns, Gusb, Hexa, Hexb, Hyal1, Igf2r, Lamp1, Lamp2, Laptm4a, Laptm4b, Laptm5, Lgmn, LipA, Man2b1, NagA, Neu1, Npc1, Pla2g15, Ppt1, Psap, Scarb2, Sgsh, Slc11a1, Slc11a2, Slc17a5, Sort1, Tcirg1	5.08E-08	3.30E-07
2	mmu04510: Focal adhesion	Actb, Actn1, Akt1, Akt3, Arhgap5, Bcar1, Bcl2, Birc2, Birc3, Capn2, Cav2, Ccnd2, Ccnd3, Cdc42, Col1a1, Col2a1, Col4a1, Col4a2, Col4a6, Col5a1, Col5a3, Diap1, Dock1, Egf, Flna, Flnb, Flnc, Fyn, Grb2, Grlf1, Gsk3b, Igf1, Igf1r, Itga2, Itga4, Itga5, Itga6, Itga7, Itga8, Itga9, Itgav, Itgb3, Itgb5, Itgb7, Kdr, Lama5, Lamb1, Lamc1, Map2k1, Mapk9, Met, Myl10, Myl12a, Mylk, Pak1, Pak2, Parvb, Parvg, Pdgfc, Pgf, Pik3cb, Pik3cd, Pik3cg, Pik3r1, Pik3r3, Pik3r5, Pip5k1c, Ppp1r12a, Prkca, Prkcb, Pten, Ptk2, Pxn, Rap1a, Rapgef1, Rasgrf1, Rock2, Shc1, Shc2, Shc4, Spp1, Src, Tln1, Tln2, Tnr, Vav1, Vav2, Vav3, Vcl, Vegfa, Vwf, Zyx	1.27E-07	8.24E-07
3	mmu04144: Endocytosis	Acap2, Acvr1b7, Adrb2, Adrbk1, Agap1, Ap2m1, Arap1, Arap3, Arf6, Arrb1, Asap1, Asap3, Cbl, Cblb, Cdc42, Chmp3, Chmp4b, Chmp6, Clta, Cltb, Cltc, Csf1r, Cxcr2, Cxcr4, Dab2, Dnm1, Dnm2, Dnm3, Eea1, Egf, Ehd1, Ehd2, Ehd4, Epn1, Epn2, Eps15, Fgfr2, Fgfr4, Git1, Glit2, Grk5, Grk6, H2-D1, H2-K1, H2-Q6, H2-Q9, H2-T3, Hspa1a, Igf1r, Il2ra, Iqsec1, Itch, Kdr, Met, Mvb12b, Nedd4l, Ntrk1, Pard3, Pard6b, Pip4k2b, Pip5k1a, Pip5k1b, Pip5k1c, Pld1, Prkcz, Psd, Psd3, Psd4, Rab11a, Rab11b, Rab11fip1, Rab11fip2, Rab11fip5, Rab22a, Rab31, Rab5b, Rab5c, Rabep1, Sh3gl1, Sh3gl3, Sh3glb1, Sh3kbp1, Smap2, Smurf1, Src, Tfrc, Tgfbr1, Tgfbr2, Tsg101, Vps37b, Vps37C, Vps45, Vps4b	4.54E-07	2.94E-06
4	mmu04666: Fc gamma R-mediated phagocytosis	Akt1, Akt3, Arf6, Arpc1b, Arpc2, Arpc4, Arpc5l, Asap1, Asap3, Cdc42, Dnm1, Dnm2, Dnm3, Fcgr1, Fcgr2b, Gab2, HCck, Igh, Inpp5d, Limk1, Limk2, Lyn, Map2k1, Myo10, Ncf1, Pak1, Pik3cb, Pik3cd, Pik3cg, Pik3r1, Pik3r3, Pik3r5, Pip4k2b, Pip5k1a, Pip5k1b, Pip5k1c, Pla2g4a, Pla2g6, Plcg2, Pld1, Ppap2a, Ppap2b, Prkca, Prkcb, Prkcd, Prkce, Ptprc, Scin, Sphk2, Syk, Vav1, Vav1, Vav3, Wasf2	5.03E-07	3.26E-06
5	mmu04010: MAPK signaling pathway	Acvr1b, Akt1, Akt3, Arrb1, Atf2, B230120H23Rik, Cacna1a, Cacna1b, Cacna1d, Cacna1f, Cacna1g, Cacna2d3, Cacnb2, Cacnb4, Cacng2, Cacng4, Casp3, Cdc42, Chuk, Dusp16, Dusp2, Dusp3, Dusp4, Dusp5, Dusp6, Egf, Fas, Fgf14, Fgf18, Fgfr1, Fgfr2, Fgfr4, Flna, Flnb, Flnc, Gadd45a, Gna12, Gng12, Grb2, Hspa1a, Ikbkb, Il1a, Il1r1, Il1r2, Map2k1, Map2k3, Map2k6, Map3k1, Map3k11, Map3k12, Map3k13, Map3k14, Map3k2, Map3k3, Map3k5, Map3k7, Map4k2, Map4k3, Map4k4, Mapk14, Mapk9, Mapkapk2, Mapt, Max, Mef2c, Mknk1, Mras, Myc, Nf1, Nfatc2, Nfatc4, Nfkb1, Nr4a1, Ntrk1, Pak1, Pak2, Pla2g12a, Pla2g2e, Pla2g4a, Pla2g5, Pla2g6, Ppm1a, Ppm1b, Ppp3ca, Ppp5c, Prkaca, Prkca, Prkcb, Ptpn5, Ptpn7, Rap1a, Rapgef2, Rasgrf1, Rasgrf2, Rasgrp1, Rasgrp3, Rps6ka2, Rps6ka4, Rps6ka5, Rras2, Srf, Stk3, Tab2, Taok3, Tgfb1, Tgfb2, Tgfbr1, Tgfbr2, Tm4sf19, Tnfrsf1a	6.23E-06	4.04E-05
6	mmu04810: Regulation of actin cytoskeleton	Abi2, Actb, Actn1, Arhgef12, Arhgef6, Arhgef7, Arpc1b, Arpc2, Arpc4, Arpc5l, Baiap2, Bcar1, Cdc42, Chrm3, Csk, Cyfip1, Cyfip2, Diap1, Diap2, Diap3, Dock1, Egf, Fgd1, Fgd3, Fgf14, Fgf18, Fgfr1, Fgfr2, Fgfr4, Git1, Gna12, Gng12, Iqgap1, Iqgap3, Itga2, Itga4, Itga5, Itga6, Itga7, Itga8, Itga9, Itgad, Itgae, Itgam, Itgav, Itgax, Itgb3, Itgb5, Itgb7, Limk1, Limk2, Map2k1, Mras, Msn, Myh10, Myh14, Myh9, Myl10, Myl12a, Mylk, Nckap1, Nckap1l, Pak1, Pak2, Pdgfc, Pik3cb, Pik3cd, Pik3cg, Pik3r1, Pik3r3, Pik3r5, Pip4k2b, Pip5k1a, Pip5k1b, Pip5k1c, Ppp1r12a, Ptk2, Pxn, Rock2, Rras2, Scin, Ssh1, Ssh2, Tiam1, Tmsb4x, Vav1, Vav2, Vav3, Vcl, Wasf2	1.38E-04	8.96E-04
7	mmu05200: Pathways in cancer	Abl1, Acvr1b, Akt1, Akt3, Arnt, Arnt2, Axin1, Bcl2, Bcl2l1, Bcr, Bid, Birc2, Birc3, Casp3, Casp8, Casp9, Cbl, Cblb, Ccdc6, Ccne1, Cdc42, Cdk6, Cdkn1a, Cdkn1b, Chuk, Col4a1, Col4a2, Col4a6, Crebbp, Csf1r, Csf3r, Ctbp2, Ctnna2, Dapk1, Dapk2, E2f1, Egf, Egln3, Epas1, Fas, Fgf14, Fgf18, Fgfr1, Fgfr2, Flt3, Fzd3, Gli2, Grb2, Gsk3b, Hsp90ab1, Igf1, Igf1r, Ikbkb, Itga2, Itga6, Itgav, Jak1, Lama5, Lamb1, Lamc1, Lef1, Map2k1, Mapk9, Max, Met, Mitf, Msh3, Msh6, Myc, Nfkb1, Ntrk1, Pax8, Pgf, Pias1, Pik3cb, Pik3cd, Pik3cg, Pik3r1, Pik3r3, Pik3r5, Plcg2, Pml, Ppard, Pparg, Prkca, Prkcb, Pten, Ptk2, Ralb, Ralgds, Rara, Rassf1, Rassf5, Rb1, Runx1, Rxra, Rxrb, Spi1, Skp2, Slc2a1, Smad3, Smo, Stat1, Stat3, Stat5a, Stat5b, SufU, Tceb1, Tcf7l2, Tfg, Tgfb1, Tgfb2, Tgfbr1, Tgfbr2, Tpm3, Traf1, Traf3, Traf5, Vegefa, Wnt1, Wnt2b, Wnt5b, Wnt7b, Zbtb16	1.39E-04	8.99E-04

(*Continued*)

Table 2. (*Continued*)

RANK	CATEGORY	FOCUSED GENES IN THE PATHWAY	*P*-VALUE CORRECTED BY BONFERRONI	FDR
8	mmu04662: B cell receptor signaling pathway	Akt1, Akt3, Blnk, Btk, Card11, Cd72, Cd81, Chuk, Dapp1, Fcgr2b, Grb2, Gsk3b, Igh, Ikbkb, Inpp5d, Lyn, Map2k1, Nfat5, Nfatc1, Nfatc2, Nfatc3, Nfatc4, Nfkb1, Nfkbie, Pik3ap1, Pik3cb, Pik3cd, Pik3cg, Pik3r1, Pik3r3, Pik3r5, Pirb, Plcg2, Ppp3ca, Prkcb, Ptpn6, Rasgrp3, Syk, Tm4sf19, Vav1, Vav2, Vav3	2.18E-04	0.001413938
9	mmu04210: Apoptosis	Akt1, Akt3, Apaf1, Atm, Bcl2, Bcl2l1, Bid, Birc2, Birc3, Capn2, Casp3, Casp7, Casp8, Casp9, Cflar, Chuk, Csf2rb, Csf2rb2, Endod1, Fas, Ikbkb, Il1a, Il1r1, Il1rap, Irak2, Irak3, Irak4, Map3k14, Myd88, Nfkb1, Ntrk1, Pik3cb, Pik3cd, Pik3cg, Pik3r1, Pik3r3, Pik3r5, Ppp3ca, Prkaca, Prkar1b, Prkar2a, Prkar2b, Tm4sf19, Tnfrsf1A	4.23E-04	0.002744042
10	mmu05222: Small cell lung cancer	Akt1, Akt3, Apaf1, Bcl2, Bcl2l1, Birc2, Birc3, Casp9, Ccne1, Cdk6, Cdkn1b, Chuk, Col4a1, Col4a2, Col4a6, E2f1, Fhit, Ikbkb, Itga2, Itga6, Itgav, Lama5, Lamb1, Lamc1, Max, Myc, Nfkb1, Pias1, Pik3cb, Pik3cd, Plik3cg, Pik3r1, Pik3r3, Pik3r5, Pten, Ptk2, Rb1, Rxra, Rxrb, Skp2, Traf1, Traf3, Traf5	5.60E-04	0.003631259
11	mmu04670: Leukocyte transendothelial migration	Actb, Actn1, Arhgap5, Bcar1, Cdc42, Cldn14, Cldn23, Ctnna2, Ctnnd1, Cxcr4, Cyba, Cybb, Esam, F11r, Gnai2, Gnai3, Grlf1, Icam1, Itga4, Itgam, Jam3, Mapk14, Mllt4, Msn, Myl10, Myl12a, Ncf1, Ncf2, Ncf4, Nox1, Pecam1, Pik3cb, Pik3cd, Pik3cg, Pik3r1, Pik3r3, Pik3r5, Plcg2, Prkca, Prkcb, Ptk2, Ptk2b, Ptpn11, Pxn, Rap1a, Rapgef4, Rassf5, Rock2, Sipa1, Txk, Vav1, Vav2, Vav3, Vcam1, Vcl	6.57E-04	0.004260774
12	mmu04062: Chemokine signaling pathway	Adcy3, Adcy7, Adrbk1, Akt1, Akt3, Arrb1, Bcar1, Ccl1, Ccl2, Ccl3, Ccl4, Ccl5, Ccl9, Ccr1, Ccr6, Cdc42, Chuk, Csk, Cx3cl1, Cx3cr1, Cxcr2, Cxcr3, Cxcr4, Elmo1, Fgr, Foxo3, Gnai2, Gnai3, Gnb1, Gng12, Gng2, Gng4, Gngt2, Grb2, Grk5, Grk6, Gsk3a, Gsk3b, Hck, Ikbkb, Lyn, Map2k1, Ncf1, Nfkb1, Pak1, Pard3, Pf4, Pik3cb, Pik3cd, Pik3cg, Pik3r1, Pik3r3, Pik3r5, Plcb2, Plcb4, Prex1, Prkaca, Prkcb, Prkcd, Prkcz, Ptk2, Ptk2b, Pxn, Rap1a, Rock2, Shc1, Shc2, Shc4, Stat1, Stat3, Stat5b, Tiam1, Vav1, Vav2, Vav3, Xcr1	8.52E-04	0.005526401
13	mmu05220: Chronic myeloid leukemia	Abl1, Acvr1b, Akt1, Akt3, Bcl2l1, Bcr, Cbl, Cblb, Cdk6, Cdkn1a, Cdkn1b, Chhuk, Ctbp2, E2f1, Gab2, GRrb2, Ikbkb, Map2k1, Myc, Nfkb1, Pik3cb, Pik3cd, Pik3cg, Pik3r1, Pik3r3, Pik3r5, Ptpn11, Rb1, Runx1, Shc1, Shc2, Shc4, Smad3, Stat5a, Stat5b, Tgfb1, Tgfb2, Tgfbr1, Tgfbr2	0.001156477	0.007503174
14	mmu04070: Phosphatidylinositol signaling system	Calm1, Calm3, Cds2, Dgkd, Dgkg, Dgki, Dgkz, Inpp4a, Inpp5a, Inpp5d, Inpp5k, Itpk1, Itpkb, Itpr1, Itpr2, Itpr3, Ocrl, Pl4kb, Pik3c2a, Pik3c2b, Pik3cb, Pik3cd, Pik3cg, Pik3r1, Pik3r3, Pik3r5, Pip4k2b, Pip5k1a, Pip5k1b, Pip5k1c, Plcb2, Plcb4, Plcd3, Plce1, Plcg2, Prkca, Prkcb, Pten, Synj1	0.002271981	0.014748224
15	mmu04660: T cell receptor signaling pathway	Akt1, Akt3, Card11, Cbl, Cblb, Cd247, Cd28, Cd4, Cdc42, Chuk, Ctla4, Fyn, Grap2, Grb2, Gsk3b, Icos, Ikbkb, Il10, Il4, Lcp2, Map2Kk1, Map3k14, Map3k7, Mapk14, Mapk9, Nck1, Nck2, Nfat5, Nfatc1, Nfatc2, Nfatc3, Nfatc4, Nfkb1, Nfkbie, Pak1, Pak2, Pdk1, Pik3cb, Pik3cd, Pik3cg, Pik3r1, Pik3r3, Pik3r5, Ppp3ca, Prkcq, PtpnN6, Ptprc, Rasgrp1, Tec, Tm4sf19, Vav1, Vav2, Vav3	0.002792449	0.018131185
16	mmu05212: Pancreatic cancer	Acvr1b, Akt1, Akt3, Arhgef6, Bcl2l1, Casp9, Cdc42, Cdk6, Chuk, E2f1, Egf, Ikbkb, Jak1, Map2k1, Mapk9, Nfkb1, Pgf, Pik3cb, Pik3cd, Pik3cg, Pik3r1, Pik3r3, Pik3r5, Pld1, Ralb, Ralgds, Rb1, Smad3, Stat1, Stat3, Tgfb1, Tgfb2, Tgfbr1, Tgfbr2, Vegfa	0.015811557	0.103295105
17	mmu04650: Natural killer cell mediated cytotoxicity	Bid, Casp3, Cd244, Cd247, Fas, Fcgr3, Fcgr4, Fyn, Grb2, H2-D1, H2-K1, Hcst, Icam1, Icam2, Ifnab, Ifngr1, Ifngr2, Igh, Klrb1c, Lcp2, Map2k1, Nfat5, Nfatc1, Nfatc2, Nfatc3, Nfatc4, Pak1, Pik3cb, Pik3cd, Pik3cg, Pik3r1, Pik3r3, Pik3r5, Plcg2, Ppp3ca, Prkca, Prkcb, Ptk2b, Ptpn11, Ptpn6, Raet1d, Raet1e, Sh3bp2, Shc1, Shc2, Shc4, Syk, Tm4sf19, Tyrobp, Vav1, Vav2, Vav3	0.038233058	0.252464917

Notes: By importing Entrez Gene IDs of 5,264 ChIP-Seq-based Spi1 target genes into the Functional Annotation tool of DAVID, KEGG pathways showing significant relevance to the set of imported genes were identified. They are listed with pathways, focused genes, p-value corrected by Bonferroni multiple comparison test, and false discovery rate (FDR).

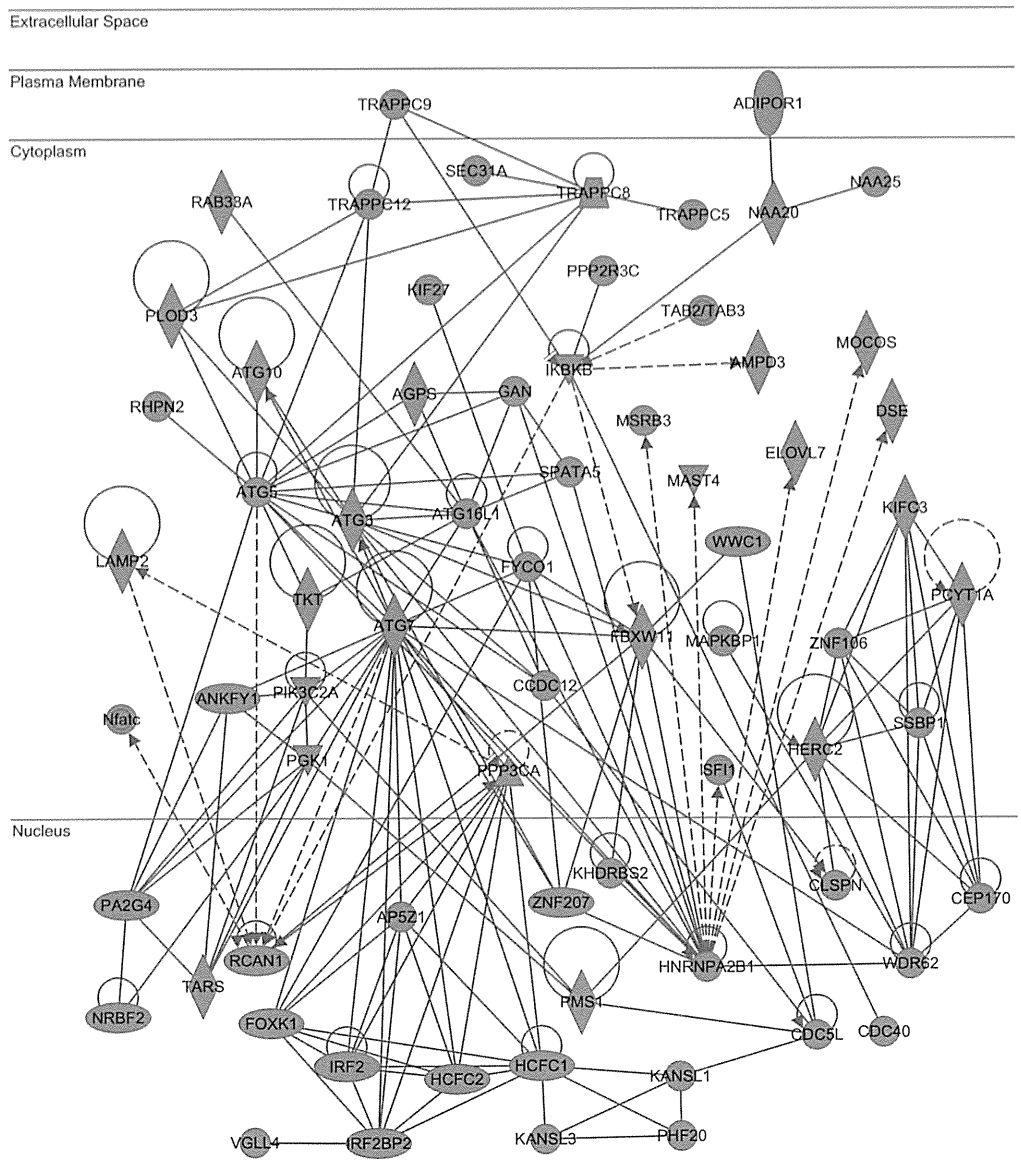

Figure 5. IPA "Cell Morphology, Cellular Function and Maintenance, Cell Death and Survival" network relevant to Spi1 target genes. Entrez Gene IDs of 5,264 ChIP-Seq-based Spi1 target genes were imported into the Core Analysis tool of IPA. It extracted the "Cell Morphology, Cellular Function and Maintenance, Cell Death and Survival" network as the first rank significant functional network as listed in Supplementary Table 3. Spi1 target genes are colored by red.

Syk as a group of Spi1 target genes, consistent partly with previous observations.[42] Importantly, Dap12 serves as a hub of the "microglial sensome" network, on which major molecular connections are concentrated.[30] These observations indicate that aberrant function of microglia plays a central role in the pathogenesis of NHD.

A recent study by combining genome-wide linkage analysis and exome sequencing identified several mutations in the *CSF1R* gene in patients with hereditary diffuse leukoencephalopathy with spheroids (HDLS), a rare autosomal dominant disease that affects predominantly the CNS white matter.[43] Clinically, HDLS exhibits early-onset personality and behavioral disturbances, dementia, and parkinsonism. HDLS shows striking similarities to the pathology of NHD, in view of diffuse demyelination and gliosis with morphologically abnormal microglia and marked accumulation of axonal spheroids, although HDLS never exhibits bone cysts and basal ganglia calcification, both of which are characteristic features of NHD. We identified *Csf1r*, *Csf1*, and *Il34* as another group of Spi1 target genes, indicating that HDLS represents a disease entity designated as "microgliopathy" caused by microglial dysfunction. Based on these observations, we could

propose a hypothesis that microglial dysfunction caused by aberrant regulation of PU.1 target genes contributes to the pathogenesis of various neurodegenerative and neuroinflammatory diseases. Importantly, a recent study indicates that DAP12 acts as a central regulator in gene networks of the late-onset AD.[44]

Although ChIP-Seq serves as a highly efficient method for genome-wide profiling of transcription factor-binding sites, the method intrinsically requires several technical considerations to achieve reproducibility of the results.[45] The specificity of antibodies, the sequencing depth and coverage, the source of target cell types and relevant controls, developmental stages, and culture conditions constitute critical factors capable of affecting both genetic and epigenetic features. Motif analysis of a defined set of high-quality peaks makes it possible to evaluate the antibody specificity and to predict the specificity of DNA–protein interaction to some extent.[45] In general, DNA-binding by transcription factors is a highly dynamic process following recruitment of the complex of auxiliary factors, such as coactivators and corepressors. However, in most occasions, ChIP-Seq data generally reflect a snapshot of binding actions of limited DNA-binding factors onto responsive elements, not always corresponding to their biological activities. Because of these limitations, it is highly important to validate main results by examining technical and biological replicates of samples with different sources of ChIP-quality antibodies, along with transcriptome analysis.

Conclusions

By analyzing a ChIP-Seq dataset numbered SRP036026 with the Strand NGS program, we identified 5,264 Spi1 target protein-coding genes in BV2 mouse microglial cells. They included *Spi1, Irf8, Runx1, Csf1r, Csf1, Il34, Aif1* (*Iba1*), *Cx3cr1, Trem2*, and *Tyrobp*. Motif analysis identified the PU-box consensus sequences in the genomic regions surrounding ChIP-Seq peaks. By using pathway analysis tools of bioinformatics, we found that ChIP-Seq-based Spi1 target genes show a significant relationship with diverse pathways essential for normal function of monocytes/macrophages, such as endocytosis, Fcγ receptor-mediated phagocytosis, and lysosomal degradation. These results suggest that PU.1/Spi1 plays a pivotal role in regulation of the genes relevant to specialized functions of microglia. Therefore, aberrant regulation of PU.1 target genes might contribute to the development of neurodegenerative diseases with accumulation of activated microglia.

Acknowledgments

The authors thank Ms. Mutsumi Motouri for her invaluable help.

Author Contributions

JS designed the methods, analyzed the data, and drafted the manuscript. NA, SK, and YK helped with the data analysis. All authors have read and approved the final manuscript.

Supplementary Materials

Supplementary Figure 1. FastQC analysis of ChIP-Seq data. FASTQ format files composed of cleaned NGS data derived from Spi1 (panel a) or Cebpa (panel b) ChIP-Seq were imported into the FastQC program. The per base sequence quality score is shown with the median (red line), the mean (blue line), and the interquartile range (yellow box).

Supplementary Figure 2. Genomic locations of Spi1 ChIP-Seq peaks on the *Trem2* gene. The genomic locations of Spi1 ChIP-Seq peaks were determined by importing the processed data into GenomeJack. An example of triggering receptor expressed on myeloid cells 2 (Trem2; Entrez Gene ID 83433) is shown, where a MACS peak numbered 51970 in the Spi1.bam Coverage lane is located in the intronic region of the *Trem2* gene (panel a) with a Spi1-binding consensus sequence motif highlighted by orange square (panel b).

Supplementary Figure 3. Genomic locations of Spi1 ChIP-Seq peaks on the *Tyrobp* gene. The genomic locations of Spi1 ChIP-Seq peaks were determined by importing the processed data into GenomeJack. An example of TYRO protein kinase binding protein (Tyrobp, Dap12; Entrez Gene ID 22177) is shown, where a MACS peak numbered 100752 in the Spi1.bam Coverage lane is located in the promoter region of the *Tyrobp* gene (panel a) with a Spi1-binding consensus sequence motif (reverse complement) highlighted by orange square (panel b).

Supplementary Figure 4. KeyMolnet molecular network relevant to Spi1 target genes. Entrez Gene IDs of 5,264 Spi1 target genes were imported into KeyMolnet. The neighboring network-search algorithm extracted the extremely complex network composed of 5,788 molecules and 13,719 molecular relations, showing the most significant relationship with "Transcriptional regulation by RB/E2F". Red nodes indicate those closely related to imported genes. White nodes exhibit additional nodes extracted automatically from the core contents of KeyMolnet to establish molecular connections. The molecular relation is indicated by solid line with arrow (direct binding or activation), solid line with arrow and stop (direct inactivation), solid line without arrow (complex formation), dash line with arrow (transcriptional activation), and dash line with arrow and stop (transcriptional repression).

Supplementary Table 1. The set of 5,264 ChIP-Seq-based Spi1 target genes in microglia. From the ChIP-Seq dataset, we identified 5,264 Spi1-target genes in BV2 mouse microglia showing fold enrichment (FE) ≥5. They are listed with the chromosome, the position of the peak (start, end), FE, Entrez Gene ID, Gene Symbol, and Gene Name. The set of 1,844 Cebpa-target genes are underlined.

Supplementary Table 2. The list of 100 microglial sensome genes. The set of 100 microglial sensome genes (Ref. 30) are listed in order of their expression levels with Entrez Gene ID, Gene Symbol, Gene Name, and an existence of ChIP-Seq-based peaks for Spi1 or Cebpa.

Supplementary Table 3. IPA functional networks relevant to ChIP-Seq-based Spi1 target genes in microglia. By importing Entrez Gene IDs of 5,264 ChIP-Seq-based Spi1 target genes into the core analysis tool of IPA, functional networks showing significant relevance to the imported genes were identified. They are listed with rank, category of functional networks, focused molecules, and *P*-value by the Fisher's exact test.

REFERENCES

1. Saijo K, Glass CK. Microglial cell origin and phenotypes in health and disease. *Nat Rev Immunol.* 2011;11(11):775–87.
2. Ginhoux F, Greter M, Leboeuf M, et al. Fate mapping analysis reveals that adult microglia derive from primitive macrophages. *Science.* 2010;330(6005):841–5.
3. Schulz C, Perdiguero EG, Wieghofer P, et al. Microglia emerge from erythromyeloid precursors via Pu.1- and Irf8-dependent pathways. *Nat Neurosci.* 2013;16(3):273–80.
4. Perry VH, Nicoll JA, Holmes C. Microglia in neurodegenerative disease. *Nat Rev Neurol.* 2010;6(4):193–201.
5. Heneka MT, Kummer MP, Latz E. Innate immune activation in neurodegenerative disease. *Nat Rev Immunol.* 2014;14(7):463–77.
6. Tahara K, Kim HD, Jin JJ, Maxwell JA, Li L, Fukuchi K. Role of toll-like receptor signalling in Ab uptake and clearance. *Brain.* 2006;129(pt 11):3006–19.
7. Halle A, Hornung V, Petzold GC, et al. The NALP3 inflammasome is involved in the innate immune response to amyloid-β. *Nat Immunol.* 2008;9(8):857–65.
8. Béraud D, Twomey M, Bloom B, et al. α-Synuclein alters toll-like receptor expression. *Front Neurosci.* 2011;5:80.
9. Crotti A, Benner C, Kerman BE, et al. Mutant Huntingtin promotes autonomous microglia activation via myeloid lineage-determining factors. *Nat Neurosci.* 2014;17(4):513–21.
10. Turkistany SA, DeKoter RP. The transcription factor PU.1 is a critical regulator of cellular communication in the immune system. *Arch Immunol Ther Exp (Warsz).* 2011;59(6):431–40.
11. Pham TH, Minderjahn J, Schmidl C, et al. Mechanisms of in vivo binding site selection of the hematopoietic master transcription factor PU.1. *Nucleic Acids Res.* 2013;41(13):6391–402.
12. McKercher SR, Torbett BE, Anderson KL, et al. Targeted disruption of the PU.1 gene results in multiple hematopoietic abnormalities. *EMBO J.* 1996;15(20):5647–58.
13. Beers DR, Henkel JS, Xiao Q, et al. Wild-type microglia extend survival in PU.1 knockout mice with familial amyotrophic lateral sclerosis. *Proc Natl Acad Sci U S A.* 2006;103(43):16021–6.
14. Smith AM, Gibbons HM, Oldfield RL, et al. M-CSF increases proliferation and phagocytosis while modulating receptor and transcription factor expression in adult human microglia. *J Neuroinflammation.* 2013;10:85.
15. Smith AM, Gibbons HM, Oldfield RL, et al. The transcription factor PU.1 is critical for viability and function of human brain microglia. *Glia.* 2013;61(6):929–42.
16. Horiuchi M, Wakayama K, Itoh A, et al. Interferon regulatory factor 8/interferon consensus sequence binding protein is a critical transcription factor for the physiological phenotype of microglia. *J Neuroinflammation.* 2012;9:227.
17. Zusso M, Methot L, Lo R, Greenhalgh AD, David S, Stifani S. Regulation of postnatal forebrain amoeboid microglial cell proliferation and development by the transcription factor Runx1. *J Neurosci.* 2012;32(33):11285–98.
18. Park PJ. ChIP-seq: advantages and challenges of a maturing technology. *Nat Rev Genet.* 2009;10(10):669–80.
19. Satoh J, Kawana N, Yamamoto Y. Pathway analysis of ChIP-Seq-based NRF1 target genes suggests a logical hypothesis of their involvement in the pathogenesis of neurodegenerative diseases. *Gene Regul Syst Bio.* 2013;7:139–52.
20. Blasi E, Barluzzi R, Bocchini V, Mazzolla R, Bistoni F. Immortalization of murine microglial cells by a v-raf/v-myc carrying retrovirus. *J Neuroimmunol.* 1990;27(2–3):229–37.
21. Zhang Y, Liu T, Meyer CA, et al. Model-based analysis of ChIP-Seq (MACS). *Genome Biol.* 2008;9(9):R137.
22. Zhang X, Robertson G, Krzywinski M, et al. PICS: probabilistic inference for ChIP-seq. *Biometrics.* 2011;67(1):151–63.
23. Li L. GADEM: a genetic algorithm guided formation of spaced dyads coupled with an EM algorithm for motif discovery. *J Comput Biol.* 2009;16(2):317–29.
24. Huang da W, Sherman BT, Lempicki RA. Systematic and integrative analysis of large gene lists using DAVID bioinformatics resources. *Nat Protoc.* 2009;4(1):44–57.
25. Kanehisa M, Goto S, Sato Y, Furumichi M, Tanabe M. KEGG for integration and interpretation of large-scale molecular data sets. *Nucleic Acids Res.* 2012;40(Database Issue):D109–14.
26. Satoh J, Tabunoki H. Comprehensive analysis of human microRNA target networks. *BioData Min.* 2011;4:17.
27. Jin H, Li L, Xu J, et al. Runx1 regulates embryonic myeloid fate choice in zebrafish through a negative feedback loop inhibiting Pu.1 expression. *Blood.* 2012;119(22):5239–49.
28. Wang Y, Szretter KJ, Vermi W, et al. IL-34 is a tissue-restricted ligand of CSF1R required for the development of Langerhans cells and microglia. *Nat Immunol.* 2012;13(8):753–60.
29. Klünemann HH, Ridha BH, Magy L, et al. The genetic causes of basal ganglia calcification, dementia, and bone cysts: DAP12 and TREM2. *Neurology.* 2005;64(9):1502–7.
30. Hickman SE, Kingery ND, Ohsumi TK, et al. The microglial sensome revealed by direct RNA sequencing. *Nat Neurosci.* 2013;16(12):1896–905.
31. Kierdorf K, Prinz M. Factors regulating microglia activation. *Front Cell Neurosci.* 2013;7:44.
32. Ginhoux F, Lim S, Hoeffel G, Low D, Huber T. Origin and differentiation of microglia. *Front Cell Neurosci.* 2013;7:45.
33. Henn A, Lund S, Hedtjärn M, Schrattenholz A, Pörzgen P, Leist M. The suitability of BV2 cells as alternative model system for primary microglia cultures or for animal experiments examining brain inflammation. *ALTEX.* 2009;26(2):83–94.
34. Rosenbauer F, Wagner K, Kutok JL, et al. Acute myeloid leukemia induced by graded reduction of a lineage-specific transcription factor, PU.1. *Nat Genet.* 2004;36(6):624–30.
35. Rekhtman N, Choe KS, Matushansky I, Murray S, Stopka T, Skoultchi AI. PU.1 and pRB interact and cooperate to repress GATA-1 and block erythroid differentiation. *Mol Cell Biol.* 2003;23(21):7460–74.
36. Chen H, Ray-Gallet D, Zhang P, et al. PU.1 (Spi-1) autoregulates its expression in myeloid cells. *Oncogene.* 1995;11(8):1549–60.
37. Wang D, D'Costa J, Civin CI, Friedman AD. C/EBPα directs monocytic commitment of primary myeloid progenitors. *Blood.* 2006;108(4):1223–9.
38. Friedman AD. C/EBPa induces PU.1 and interacts with AP-1 and NF-kB to regulate myeloid development. *Blood Cells Mol Dis.* 2007;39(3):340–3.
39. Gómez-Nicola D, Fransen NL, Suzzi S, Perry VH. Regulation of microglial proliferation during chronic neurodegeneration. *J Neurosci.* 2013;33(6):2481–93.
40. Satoh J, Tabunoki H, Ishida T, et al. Immunohistochemical characterization of microglia in Nasu-Hakola disease brains. *Neuropathology.* 2011;31(4):363–75.
41. Takahashi K, Rochford CD, Neumann H. Clearance of apoptotic neurons without inflammation by microglial triggering receptor expressed on myeloid cells–2. *J Exp Med.* 2005;201(4):647–57.
42. Weigelt K, Ernst W, Walczak Y, et al. Dap12 expression in activated microglia from retinoschisin-deficient retina and its PU.1-dependent promoter regulation. *J Leukoc Biol.* 2007;82(6):1564–74.
43. Rademakers R, Baker M, Nicholson AM, et al. Mutations in the colony stimulating factor 1 receptor (CSF1R) gene cause hereditary diffuse leukoencephalopathy with spheroids. *Nat Genet.* 2011;44(2):200–5.
44. Zhang B, Gaiteri C, Bodea LG, et al. Integrated systems approach identifies genetic nodes and networks in late-onset Alzheimer's disease. *Cell.* 2013;153(3):707–20.
45. Landt SG, Marinov GK, Kundaje A, et al. ChIP-seq guidelines and practices of the ENCODE and modENCODE consortia. *Genome Res.* 2012;22(9):1813–31.

Journal of Affective Disorders 165 (2014) 59–63

Contents lists available at ScienceDirect

Journal of Affective Disorders

journal homepage: www.elsevier.com/locate/jad

Research report

Characteristic distributions of regional cerebral blood flow changes in major depressive disorder patients: A pseudo-continuous arterial spin labeling (pCASL) study

Miho Ota [a,*], Takamasa Noda [b], Noriko Sato [c], Kotaro Hattori [a], Toshiya Teraishi [a], Hiroaki Hori [a], Anna Nagashima [a], Keigo Shimoji [c], Teruhiko Higuchi [d], Hiroshi Kunugi [a]

[a] Department of Mental Disorder Research, National Institute of Neuroscience, 4-1-1, Ogawa-Higashi, Kodaira, Tokyo, Japan
[b] Department of Psychiatry, National Institute of Neuroscience, 4-1-1, Ogawa-Higashi, Kodaira, Tokyo, Japan
[c] Department of Radiology, National Institute of Neuroscience, 4-1-1, Ogawa-Higashi, Kodaira, Tokyo, Japan
[d] National Center of Neurology and Psychiatry, National Institute of Neuroscience, 4-1-1, Ogawa-Higashi, Kodaira, Tokyo 187-8502, Japan

ARTICLE INFO

Article history:
Received 25 March 2014
Accepted 11 April 2014
Available online 21 April 2014

Keywords:
Biological parametric mapping
Cerebral blood flow
Major depressive disorder
Pseudo-continuous arterial spin labeling
Schizophrenia

ABSTRACT

Background: Most previous studies that examined regional cerebral blood flow (rCBF) abnormalities in major depressive disorder (MDD) required the injection of radioisotopes into subjects. Here by using magnetic resonance imaging (MRI) with the pseudo-continuous arterial spin labeling (pCASL) method which does not require radioisotopes, we examined rCBF in patients with MDD in comparison with that in patients with schizophrenia and healthy subjects, taking the regional cerebral gray matter volume into account.
Methods: Subjects were 27 patients with MDD, 42 with schizophrenia and 43 healthy volunteers who underwent 3-T MRI with pCASL. Obtained pCASL imaging data were subject to the voxel-by-voxel statistical analysis.
Results: There were significant reductions of rCBF in the right inferior prefrontal cortex and anterior cingulate cortices (ACCs) in the MDD patients compared with the healthy controls. When compared with the schizophrenic patients, the MDD patients showed lower rCBF in the subgenual ACC and higher rCBF in left occipital region.
Limitation: The abnormalities of rCBF in MDD were known to reverse during symptom remission. Further study with follow-up period would bring the perception about the treatment response.
Conclusion: The rCBF reduction in the subgenual region may be a specific functional abnormality to MDD patients, which may provide a biological marker for MDD. The MRI with pCASL method is a promising tool to detect rCBF abnormalities controlling for gray matter volume in psychiatric disorders.

1. Introduction

Major depressive disorder (MDD) is a common disorder, and the lifetime prevalence was reported to be 8–12% (Andrade et al., 2003). Structural brain abnormalities in areas involved in emotional processing including the dorsolateral prefrontal region, orbitofrontal region, cingulate cortex, temporal region, hippocampus and striatum have been reported in MDD (reviewed in Arnone et al., Bora et al., 2012; Murphy and Frodl, 2011; Sexton et al., 2009). Previous studies using nuclear medicine techniques such as single photon emission computed tomography (SPECT) and positron emission tomography (PET) showed significant reductions of regional cerebral blood flow (rCBF) and metabolism in the frontal, parietal, and temporal regions of patients with MDD (Drevets et al., 2002; Mayberg et al., 2000; Smith and Cavanagh, 2005).

Arterial spin labeling (ASL) magnetic resonance imaging (MRI) is a novel noninvasive (i.e., non-radioactive) technique that can measure rCBF by taking advantage of arterial water as a freely diffusible tracer. This technique has recently been applied to detect functional abnormalities of the brain in MDD patients (Duhameau et al., 2010; Ho et al., 2013; Järnum et al., 2011; Lui et al., 2009; Walther et al., 2012). Some of these studies showed rCBF reduction in the frontal regions (Ho et al., 2013; Lui et al., 2009) and anterior cingulate cortex (ACC) (Walther et al., 2012). However, the others found no significant reduction in MDD patients (Duhameau et al., 2010; Järnum et al., 2011). Importantly, the limited spatial resolution of ASL images precludes accurate rCBF measurements because

* Correspondence to: Department of Mental Disorder Research, National Institute of Neuroscience, National Center of Neurology and Psychiatry, 4-1-1, Ogawa-Higashi, Kodaira, Tokyo 187-8502, Japan. Tel.: +81 42 341 2712; fax: +81 42 346 2094.
E-mail address: ota@ncnp.go.jp (M. Ota).

http://dx.doi.org/10.1016/j.jad.2014.04.032
0165-0327/

the partial volume effects on ASL cause an underestimation of activity in small brain structures. Since many MDD patients have altered brain structures as described above, their rCBF images are likely to be influenced by the partial volume effect. To our knowledge, however, no ASL study in MDD has thus far taken account of thise partial volume effect.

In this study, we examined differences in rCBF between patients with MDD and healthy controls by a recently developed method, pseudo-continuous ASL (pCASL), taking the regional cerebral gray matter volume into account (Dai et al., 2008; Wu et al., 2007). In addition, depressive features or syndromes are often manifested in patients with schizophrenia. It has been estimated that depression is manifested in 21 to 74% of acute patients with recent onset schizophrenia and in 13 to 50% of patients with chronic schizophrenia, while depressive features have been found in even higher rates, up to 80%, in patients with schizophrenia (Kollias et al., 2008). So it would be useful if there is a method to differentiate between MDD and schizophrenia by using a neuroimaging method. We previously reported MRI-pCASL study on schizophrenia that showed a significant reduction of rCBF in the left inferior frontal cortex (Ota et al., 2014). So we evaluated rCBF of MDD patients in comparison with that of schizophrenia patients as well.

2. Methods

2.1. Participants

Subjects were 27 patients with MDD, 42 patients with schizophrenia and 43 age- and gender-matched healthy subjects. The subjects partially overlapped with those in the previous report (Ota et al., 2014). A consensus diagnosis was made according to the Diagnostic and Statistical Manual of Mental Disorders, 4th ed. (DSM-IV) criteria (American Psychiatric Association, 1994), by a research psychiatrist (MO, HH, or TT). The MDD patients were rated with Hamilton Depression Rating scale (HAM-D) for their depressive symptoms (Hamilton, 1960), and the schizophrenic patients were done with the Positive and Negative Syndrome Scale (PANSS) (Kay et al., 1987). MDD patients who were in remission, as defined by the total score on the HAM-D of less than 8, were not enrolled in the study (Mayberg et al., 2005). Daily doses of antidepressants were converted to imipramine equivalents, and daily doses of antipsychotics including depot antipsychotics were converted to chlorpromazine equivalents using published guidelines (American Psychiatric Association, 1997; Inagaki et al., 1999).

Controls were recruited from the community through local magazine advertisements and our website announcement. These participants were interviewed for enrollment by a research psychiatrist using the Japanese version of the Mini-International Neuropsychiatric Interview (Otsubo et al., 2005; Sheehan et al., 1998). Participants were excluded if they had a prior medical history of central nervous system disease or severe head injury, or if they met the criteria for substance abuse or dependence. Those individuals who demonstrated a history of psychiatric illness or contact with psychiatric services were excluded from the control group.

After the study was explained to each participant, his or her written informed consent was obtained for participation in the study. This study was approved by the ethics committee of the National Center of Neurology and Psychiatry, Japan.

2.2. MRI data acquisition and processing

Imaging was performed on a 3-T MR system (Philips Medical Systems, Best, the Netherlands). 3D T1-weighted images and pCASL images were acquired as the same parameter as described previously (Ota et al., 2014). For measurement of the magnetization of arterial blood and also for segmentation purposes, an EPI M0 image was obtained separately with the same geometry and the same imaging parameters as the pCASL without labeling.

2.3. Postprocessing of the ASL data

Because the pCASL and M0 images were acquired separately, the image signal intensities of both were corrected for data scaling. Corrected data were transferred to a workstation and analyzed using ASLtbx software (Wang et al., 2008) running on statistical parametric mapping 5 (SPM5). For the rCBF calculations, we added the attenuation correction for the transversal relaxation rate of gray matter to the original equation. Details of this process are described elsewhere (Ota et al., 2013a).

The mean rCBF image derived using the ASLtbx software contained some patchy noise, and thus we used a median filter (a nonlinear digital filtering technique). In median filtering, the neighboring pixels are ranked according to their intensity, and the median value becomes the new value for the central pixel. Since the slice gap that we used was somewhat large, simple 2D median filtering (3 voxels × 3 voxels) was used. To evaluate rCBF voxel-basically, we normalized the mean rCBF images to the standard space. First, each individual 3D-T1 image was coregistered and resliced to its own M0 image. Next, the coregistered 3D-T1 image was normalized to the "avg152T1" image regarded as the anatomically standard image using with the DARTEL (diffeomorphic anatomical registration using exponentiated lie) registration method (Ashburner, 2007). Finally, the transformation matrix was applied to the mean rCBF images treated with the median filter. The spatially normalized images were resliced with a final voxel size of approx. 4 × 4 × 8 mm. Each map was then spatially smoothed with a 4-mm full-width at half-maximum Gaussian kernel in order to decrease spatial noise and compensate for the inexactitude of normalization.

2.4. Statistical analysis

Statistical analyses were performed using SPM5 software. Differences in rCBF among 3 diagnostic groups were assessed using the age and gender as non-imaging nuisance variables and the individual normalized gray matter volume image as an imaging nuisance covariate using Biological Parametric Mapping (BPM) (Casanova et al., 2007). Only differences that met the following criteria were deemed significant: a seed level of $p < 0.05$ (false discovery rate [FDR] correction for multiple comparisons) and a cluster level of $p < 0.05$ (uncorrected).

3. Results

Demographic and clinical characteristics of the participants are shown in Table 1. There was no significant difference in age or gender among the 3 diagnostic groups.

There were significant rCBF reductions in the ACCs and right inferior prefrontal cortex in the patients with MDD compared with the controls (Fig. 1). We found significant rCBF reductions in the ACC, bilateral prefrontal cortex, left superior temporal cortex, and bilateral occipital cortex in the patients with schizophrenia compared with the controls, which is consistent with the results of our previous study (Fig. 2) (Ota et al., 2014). When the 2 patient groups were compared, the MDD patients showed significantly lower rCBF in subgenual ACC (Fig. 3A) and higher rCBF in left occipital cortex (Fig. 3B) compared with the schizophrenic patients.

Table 1
Demographic and clinical characteristics of subjects.

Variable	MDD $n=27$			Schizophrenia $n=42$			Healthy subjects $n=43$			p Value
	Mean	±	SD	Mean	±	SD	Mean	±	SD	
Gender (M:F)	13	:	14	22	:	20	21	:	22	0.93
Age (years)	38.9	±	9.9	39.2	±	11.5	37.4	±	12.7	0.75
Antidepressant medication (mg/day)[a]	####	±	75.7							
Antipsychotic medication (mg/day)[b]				627.1	±	503.0				
HAM-D	16.6	±	7.3							
PANSS total				63.4	±	18.9				

MDD; major depressive disorder.
HAM-D; Hamilton's rating scale for depression.
PANSS; positive and negative synptom scale.
[a] Impramine equivalent.
[b] Chlorpromazine equivalent.

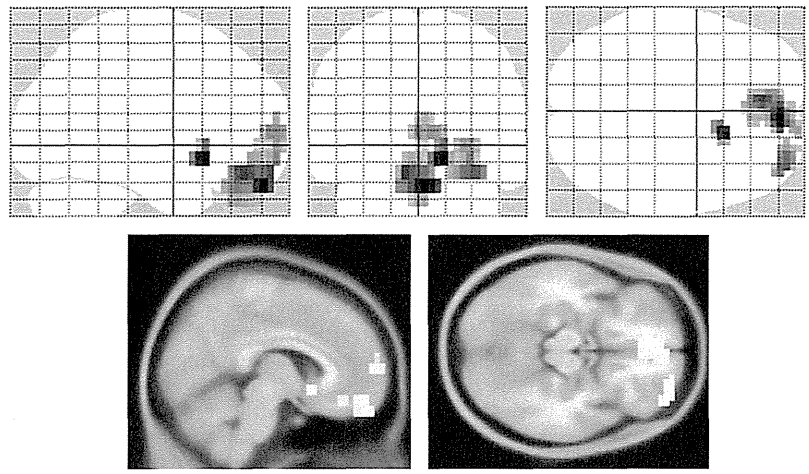

Fig. 1. Regional cerebral blood flow (rCBF) changes in major depressive disorder (MDD). There were significant reductions of rCBF in the right inferior prefrontal and anterior cingulate cortices (ACCs) compared with healthy subjects ($p < 0.05$, (false discovery rate [FDR])).

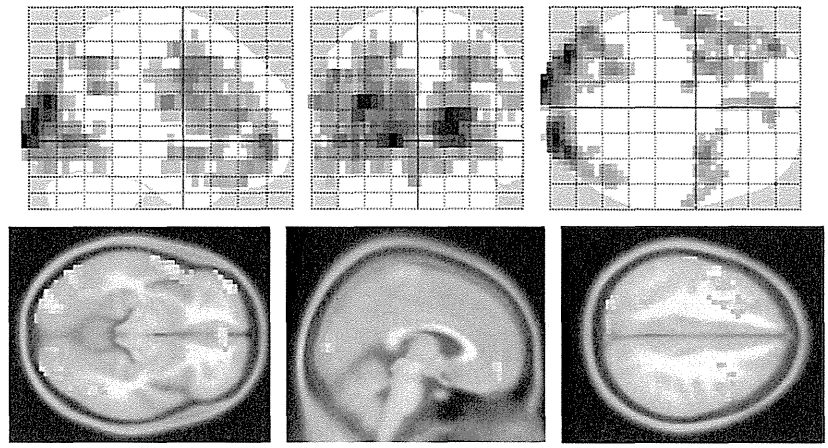

Fig. 2. Regional CBF changes in schizophrenia. There were significant reductions of rCBF in the bilateral prefrontal and occipital cortices, left temporal cortex, and ACC compared with healthy subjects ($p < 0.05$, FDR).

4. Discussion

We examined rCBF changes inMDD patients compared with healthy subjects and schizophrenia patients. By using the pCASL method and the regional gray matter volume correction, we found significant changes of rCBF in cingulate and frontal regions in MDD patients. To our knowledge, this is the first study of ASL-based rCBF changes in MDD patients that took the regional gray matter volume into account. In addition, we found differences in rCBF between MDD and schizophrenia patients by using this method.

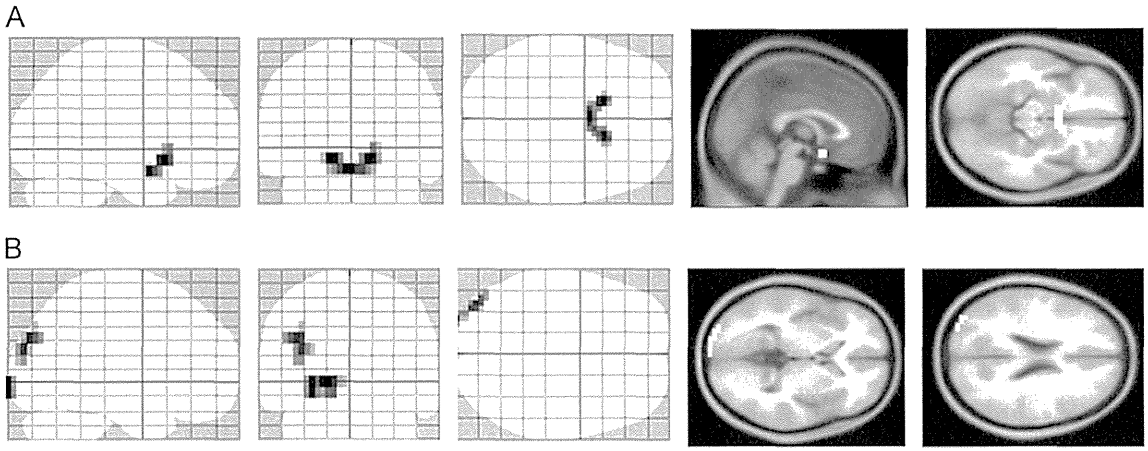

Fig. 3. Comparison of rCBF between the patients with MDD and schizophrenia. The MDD patients showed the lower rCBF in the subgenual ACC (A) and the higher rCBF in left occipital region (B) than schizophrenic patients. ($p < 0.05$, FDR).

Many MRI studies have focused on structural brain volume changes in MDD (reviewed in Arnone et al., 2012; Bora et al., 2012), and some studies have reported altered functions by using ASL (Ho et al., 2013; Lui et al., 2009; Walther et al., 2012). In addition, studies using PET and SPECT found that patients with MDD have decreased rCBF and metabolism (see review; Fitzgerald et al., 2008). We observed reduction of rCBF in the inferior prefrontal cortex in the MDD relative to healthy subjects. These findings mirror previous ASL studies showing lower baseline frontal rCBF (Ho et al., 2013; Lui et al., 2009; Walther et al., 2012). Hypoactivity in frontal areas has been strongly linked to psychomotor retardation (Galynker et al., 1998; Bench et al., 1992), and impaired executive functioning (e.g., attention, working memory, and decision making) (Paelecke-Habermann et al., 2005; Fossati et al., 2002). Together with findings from these studies, our results suggest that reduced perfusion in these regions may be associated with some of the cognitive and motor symptoms found in MDD. Our finding of hypoperfusion in the ACC of MDD patients is consistent with several perfusion and metabolism studies of MDD (Fitzgerald et al., 2008; Ho et al., 2013; Walther et al., 2012). The ACC has been shown to be involved in the processing of emotion and motivation (Carter et al., 1999). Thus, dysfunction in the ACC may underlie some of the core affective symptoms seen in MDD. Specifically, previous studies have shown that there were structural (Coryell et al., 2005; Costafreda et al., 2009; Lee et al., 2011; Wagner et al., 2011) and functional (Drevets et al., 1997; Liotti et al., 2002) dysfunctions in the subgenual ACC of MDD. And some studies showed that such change in the subgenual ACC was noticeable not in schizophrenia but in MDD, compared with healthy subjects (Coryell et al., 2005; Ota et al., 2013b). In line, we detected the lower rCBF in the subgenual ACC of MDD patients than schizophrenic patients, which is consistent with the preceding results.

ASL studies of schizophrenia revealed several rCBF changes (Horn et al., 2009; Pinkham et al., 2011; Scheef et al., 2010; Walther et al., 2011). However, the results of these studies differ substantially. For the frontal and temporal cortices, three and two out of these four studies consistently reported reduced rCBF, which is compatible with our results. We found rCBF reduction in bilateral occipital cortices of the individuals with schizophrenia, which is consistent with the study by Pinkham et al. (2011) in medicated schizophrenic patients and the study by Scheef et al. (2010) in drug-free subjects. Several studies obtained evidence of deficits of schizophrenia in visual processing, using electroencephalography (EEG) (Butler et al., 2001, 2005; Doniger et al., 2002), and other studies documented the abnormal EEG activities in the occipital lobe of patients with schizophrenia (Spencer et al., 2003, 2004). Thus, it seems likely that the occipital lobe is involved in some aspects of the pathophysiology of schizophrenia.

There was limitation in this study. The abnormalities of rCBF in MDD were known to reverse during symptom remission (see review; Drevets, 2000). Our MDD patients showed the HAM-D score of > 8, depressed non-remitters, and they showed the lower rCBF than healthy subjects. Further study with follow-up period that provides the information about the response to therapy would bring the prediction about the treatment response.

In conclusion, our pCASL study with partial volume effect correction demonstrated hypoactivity in the right inferior prefrontal area and cingulate cortex in MDD patients. The rCBF reduction in the subgenual region was specific in MDD patients compared with not only the healthy subjects, but also with schizophrenic patients. This point may provide objective biological information pertaining to the clinical diagnosis of schizophrenia and MDD. Finally, the present study demonstrate that the MRI with pCASL method is a promising tool to detect rCBF abnormalities controlling for gray matter volume in psychiatric disorders.

Role of funding source

The founding source had no involvement.

Conflict of interest

All authors declare that they have no conflicts of interest.

Acknowledgement

This study was supported by Health and Labor Sciences Research Grant (Comprehensive Research on Disability, Health, and Welfare) (M.O. and H.K.), Intramural Research Grant (24-11) for Neurological and Psychiatric Disorders of NCNP (M.O. and H.K.), and "Understanding of molecular and environmental bases for brain health" carried out under the Strategic Research Program for Brain Sciences by the Ministry of Education, Culture, Sports, Science and Technology of Japan (H.K.).

References

American Psychiatric Association, 1994. DSM-IV: Diagnostic and Statistical Manual of Mental Disorders, fourth ed. Washington, DC: American Psychiatric Press, Washington, DC.

American Psychiatric Association, 1997. Practice Guidelines for the Treatment of Patients with Schizophrenia. Washington, DC: American Psychiatric Press, Washington, DC..

Andrade, L., Caraveo-Anduaga, J.J., Berglund, P., Bijl, R.V., De Graaf, R., Vollebergh, W., Dragomirecka, E., Kohn, R., Keller, M., Kessler, R.C., Kawakami, N., Kiliç, C., Offord, D., Ustun, T.B., Wittchen, H.U., 2003. The epidemiology of major

depressive episodes: results from the International Consortium of Psychiatric Epidemiology (ICPE) Surveys. Int. J. Methods Psychiatr. Res 12, 3–21.
Arnone, D., McIntosh, A.M., Ebmeier, K.P., Munafò, M.R., Anderson, I.M., 2012. Magnetic resonance imaging studies in unipolar depression: systematic review and meta-regression analyses. Eur. Neuropsychopharmacol. 22, 1–16.
Ashburner, J., 2007. A fast diffeomorphic image registration algorithm. NeuroImage 38, 95–113.
Bench, C.J., Friston, K.J., Brown, R.G., Scott, L.C., Frackowiak, R.S., Dolan, R.J., 1992. The anatomy of melancholia—focal abnormalities of cerebral blood flow in major depression. Psychol. Med. 22, 607–615.
Bora, E., Harrison, B.J., Davey, C.G., Yücel, M., Pantelis, C., 2012. Meta-analysis of volumetric abnormalities in cortico-striatal–pallidal-thalamic circuits in major depressive disorder. Psychol. Med. 42, 671–681.
Butler, P.D., Schechter, I., Zemon, V., Schwartz, S.G., Greenstein, V.C., Gordon, J., Schroeder, C.E., Javitt, D.C., 2001. Dysfunction of early-stage visual processing in schizophrenia. Am. J. Psychiatry 158, 1126–1133.
Butler, P.D., Zemon, V., Schechter, I., Saperstein, A.M., Hoptman, M.J., Lim, K.O., Revheim, N., Silipo, G., Javitt, D.C., 2005. Early-stage visual processing and cortical amplification deficits in schizophrenia. Arch. Gen. Psychiatry 62, 495–504.
Carter, C.S., Botvinick, M.M., Cohen, J.D., 1999. The contribution of the anterior cingulate cortex to executive processes in cognition. Rev. Neurosci. 10, 49–57.
Casanova, R., Srikanth, R., Baer, A., Laurienti, P.J., Burdette, J.H., Hayasaka, S., Flowers, L., Wood, F., Maldjian, J.A., 2007. Biological parametric mapping: a statistical toolbox for multimodality brain image analysis. NeuroImage 34, 137–143.
Coryell, W., Nopoulos, P., Drevets, W., Wilson, T., Andreasen, N.C., 2005. Subgenual prefrontal cortex volumes in major depressive disorder and schizophrenia: diagnostic specificity and prognostic implications. Am. J. Psychiatry 162, 1706–1712.
Costafreda, S.G., Chu, C., Ashburner, J., Fu, C.H., 2009. Prognostic and diagnostic potential of the structural neuroanatomy of depression. PLoS One 4, e6353.
Dai, W., Garcia, D., de Bazelaire, C., Alsop, D.C., 2008. Continuous flow-driven inversion for arterial spin labeling using pulsed radio frequency and gradient fields. Magn. Reson. Med. 60, 1488–1497.
Doniger, G.M., Foxe, J.J., Murray, M.M., Higgins, B.A., Javitt, D.C., 2002. Impaired visual object recognition and dorsal/ventral stream interaction in schizophrenia. Arch. Gen. Psychiatry 59, 1011–1020.
Drevets, W.C., Price, J.L., Simpson Jr., J.R., Todd, R.D., Reich, T., Vannier, M., Raichle, M.E., 1997. Subgenual prefrontal cortex abnormalities in mood disorders. Nature 386, 824–827.
Drevets, W.C., 2000. Neuroimaging studies of mood disorders. Biol. Psychiatry 48, 813–829.
Drevets, W.C., Bogers, W., Raichle, M.E., 2002. Functional anatomicalcorrelates of antidepressant drug treatment assessed using PET measures of regional glucose metabolism. Eur. Neuropsychopharmacol. 12, 527–544.
Duhameau, B., Ferré, J.C., Jannin, P., Gauvrit, J.Y., Vérin, M., Millet, B., Drapier, D., 2010. Chronic and treatment-resistant depression: a study using arterial spin labeling perfusion MRI at 3 T. Psychiatry Res. 182, 111–116.
Fitzgerald, P.B., Laird, A.R., Maller, J., Daskalakis, Z.J., 2008. A meta-analytic study of changes in brain activation in depression. Hum. Brain Mapp. 29, 683–695.
Fossati, P., Ergis, A.M, Allilaire, J.F., 2002. Executive functioning in unipolar depression: a review. L'Encephale 28, 97–107.
Galynker, I.I., Cai, J., Ongseng, F., Finestone, H., Dutta, E., Serseni, D., 1998. Hypofrontality and negative symptoms in major depressive disorder. J. Nucl. Med. 39, 608–612.
Hamilton, M., 1960. A rating scale of depression. J. Neurol. Neurosurg. Psychiatry 23, 56–62.
Ho, T.C., Wu, J., Shin, D.D., Liu, T.T., Tapert, S.F., Yang, G., Connolly, C.G., Frank, G.K., Max, J.E., Wolkowitz, O., Eisendrath, S., Hoeft, F., Banerjee, D., Hood, K., Hendren, R.L., Paulus, M.P., Simmons, A.N., Yang, T.T., 2013. Altered cerebral perfusion in executive, affective, and motor networks during adolescent depression. J. Am. Acad. Child Adolesc. Psychiatry 52, 1076–1091.
Horn, H., Federspiel, A., Wirth, M., Müller, T.J., Wiest, R., Wang, J.J., Strik, W., 2009. Structural and metabolic changes in language areas linked to formal thought disorder. Br. J. Psychiatry 194, 130–138.
Inagaki, A., Inada, T., Fujii, Y., Yagi, G., 1999. Equivalent Dose of Psychotropics. Tokyo: Seiwa Shoten.
Järnum, H., Eskildsen, S.F., Steffensen, E.G., Lundbye-Christensen, S., Simonsen, C.W., Thomsen, I.S., Fründ, E.T., Théberge, J., Larsson, E.M., 2011. Longitudinal MRI study of cortical thickness, perfusion, and metabolite levels in major depressive disorder. Acta Psychiatr. Scand. 124, 435–446.
Kay, S.R., Opler, L.A., Fiszbein, A., 1987. Positive and negative syndrome scale (PANSS) manual. Schizophr. Bull. 13, 261–276.
Kollias, C.T., Kontaxakis, V.P., Havaki-Kontaxaki, B.J., Stamouli, S., Margariti, M., Petridou, E., 2008. Association of physical and social anhedonia with depression in the acute phase of schizophrenia. Psychopathology 41, 365–370.
Lee, H.Y., Tae, W.S., Yoon, H.K., Lee, B.T., Paik, J.W., Son, K.R., Oh, Y.W., Lee, M.S., Ham, B.J., 2011. Demonstration of decreased gray matter concentration in the midbrain encompassing the dorsal raphe nucleus and the limbic subcortical regions in major depressive disorder: an optimized voxel-based morphometry study. J. Affect. Disord. 133, 128–136.
Liotti, M., Mayberg, H.S., McGinnis, S., Brannan, S.L., Jerabek, P., 2002. Unmasking disease-specific cerebral blood flow abnormalities: mood challenge in patients with remitted unipolar depression. Am. J. Psychiatry 159, 1830–1840.
Lui, S., Parkes, L.M., Huang, X., Zou, K., Chan, R.C., Yang, H., Zou, L., Li, D., Tang, H., Zhang, T., Li, X., Wei, Y., Chen, L., Sun, X., Kemp, G.J., Gong, Q.Y., 2009. Depressive disorders: focally altered cerebral perfusion measured with arterial spin-labeling MR imaging. Radiology 251, 476–484.
Mayberg, H.S., Brannan, S.K., Tekell, J.L., Silva, J.A., Mahurin, R.K., McGinnis, S., Jerabek, P.A., 2000. Regional metabolic effects of fluoxetine in major depression: serial changes and relationship to clinical response. Biol. Psychiatry 48, 830–843.
Mayberg, H.S., Lozano, A.M., Voon, V., McNeely, H.E., Seminowicz, D., Hamani, C., Schwalb, J.M., Kennedy, S.H., 2005. Deep brain stimulation for treatment-resistant depression. Neuron 45, 651–660.
Murphy, M.L., Frodl, T., 2011. Meta-analysis of diffusion tensor imaging studies shows altered fractional anisotropy occurring in distinct brain areas in association with depression. Biol. Mood Anxiety Disord 1, 3.
Ota, M., Sato, N., Nakata, Y., Ito, K., Kamiya, K., Maikusa, N., Ogawa, M., Okamoto, T., Obu, S., Noda, T., Araki, M., Yamamura, T., Kunugi, H., 2013a. Abnormalities of cerebral blood flow in multiple sclerosis: a pseudo-continuous arterial spin labeling MRI study. Magn. Reson. Imaging 31, 990–995.
Ota, M., Ishikawa, M., Sato, N., Hori, H., Sasayama, D., Hattori, K., Teraishi, T., Noda, T., Obu, S., Nakata, Y., Higuchi, T., Kunugi, H., 2013b. Discrimination between schizophrenia and major depressive disorder by magnetic resonance imaging of the female brain. J. Psychiatr. Res. 47, 1383–1388.
Ota, M., Ishikawa, M., Sato, N., Okazaki, M., Maikusa, N., Hori, H., Hattori, K., Teraishi, T., Ito, K., Kunugi, H., 2014. Pseudo-continuous arterial spin labeling MRI study of schizophrenic patients. Schizophr. Res. 154, 113–118.
Otsubo, T., Tanaka, K., Koda, R., Shinoda, J., Sano, N., Tanaka, S., 2005. Reliability and validity of Japanese version of the Mini-International Neuropsychiatric Interview. Psychiatry Clin. Neurosci. 59, 517–526.
Paelecke-Habermann, Y., Pohl, J., Leplow, B., 2005. Attention and executive functions in remitted major depression patients. J. Affect. Disord. 89, 125–135.
Pinkham, A., Loughead, J., Ruparel, K., Wu, W.C., Overton, E., Gur, R., Gur, R., 2011. Resting quantitative cerebral blood flow in schizophrenia measured by pulsed arterial spin labeling perfusion MRI. Psychiatry Res. 194, 64–72.
Scheef, L., Manka, C., Daamen, M., Kühn, K.U., Maier, W., Schild, H.H., Jessen, F., 2010. Resting-state perfusion in nonmedicated schizophrenic patients: a continuous arterial spin-labeling 3.0-T MR study. Radiology 256, 253–260.
Sexton, C.E., Mackay, C.E., Ebmeier, K.P., 2009. A systematic review of diffusion tensor imaging studies in affective disorders. Biol. Psychiatry 66, 814–823.
Sheehan, D.V., Lecrubier, Y., Sheehan, K.H., Amorim, P., Janavs, J., Weiller, E., Hergueta, T., Baker, R., Dunbar, G.C., 1998. The Mini-International Neuropsychiatric Interview (M.I.N.I.): the development and validation of a structured diagnostic psychiatric interview for DSM-IV and ICD-10. J. Clin. Psychiatry 59, 22–57.
Smith, D.J., Cavanagh, J.T., 2005. The use of single photon emission computed tomography in depressive disorders. Nucl. Med. Commun. 26, 197–203.
Spencer, K.M., Nestor, P.G., Niznikiewicz, M.A., Salisbury, D.F., Shenton, M.E., McCarley, R.W., 2003. Abnormal neural synchrony in schizophrenia. J. Neurosci. 23, 7407–7411.
Spencer, K.M., Nestor, P.G., Perlmutter, R., Niznikiewicz, M.A., Klump, M.C., Frumin, M., Shenton, M.E., McCarley, R.W., 2004. Neural synchrony indexes disordered perception and cognition in schizophrenia. Proc. Nat. Acad. Sci. U.S.A 101, 17288–17293.
Wagner, G., Koch, K., Schachtzabel, C., Schultz, C.C., Sauer, H., Schlosser, R.G., 2011. Structural brain alterations in patients with major depressive disorder and high risk for suicide: evidence for a distinct neurobiological entity? NeuroImage 54, 1607–1614.
Walther, S., Federspiel, A., Horn, H., Razavi, N., Wiest, R., Dierks, T., Strik, W., Müller, T.J., 2011. Resting state cerebral blood flow and objective motor activity reveal basal ganglia dysfunction in schizophrenia. Psychiatry Res. 192, 117–124.
Walther, S., Hofle, O., Federspiel, A., Horn, H., Hügli, S., Wiest, R., Strik, W., Müller, T. J., 2012. Neural correlates of disbalanced motor control in major depression. J. Affect. Disord. 136, 124–133.
Wang, Z., Aguirre, G.K., Rao, H., Wang, J., Fernández-Seara, M.A., Childress, A.R., Detre, J.A., 2008. Empirical optimization of ASL data analysis using an ASL data processing toolbox: ASLtbx. Magn. Reson. Imaging 26, 261–269.
Wu, W.C., Fernandez-Seara, M., Detre, J.A., Wehrli, F.W., Wang, J., 2007. A theoretical and experimental investigation of the tagging efficiency of pseudocontinuous arterial spin labeling. Magn. Reson. Med. 58, 1020–1027.

Clinical & Experimental
Neuroimmunology

Clinical and Experimental Neuroimmunology 5 (2014) 137–148

REVIEW ARTICLE

Towards understanding the role of orphan nuclear receptor NR4A2 in Th17 cell-mediated central nervous system autoimmunity: An experimental approach using an animal model of multiple sclerosis

Shinji Oki

Department of Immunology, National Institute of Neuroscience, National Center of Neurology and Psychiatry, Tokyo, Japan

Correspondence
Shinji Oki, PhD, Department of Immunology, National Institute of Neuroscience, National Center of Neurology and Psychiatry, 4-1-1 Ogawahigashi, Kodaira, Tokyo 187-8502, Japan.
Tel: +81-42-341-2711
Fax: +81-42-346-1753
Email: soki@ncnp.go.jp

Received: 31 March 2014; revised: 20 April 2014; accepted: 21 April 2014.

Abstract

Although details of its pathogenesis remain elusive, multiple sclerosis (MS) is now widely accepted as an autoimmune disease of the central nervous system (CNS) in which autoreactive helper T cells play a pivotal role in triggering pathogenic cascades. Recently developed drugs and ongoing clinical trials clearly reflect the significance of targeting pathogenic immune cells, such as T helper 17 (Th17) cells, for MS treatment. Through comprehensive gene expression profiling analysis, we previously showed that the orphan nuclear receptor, NR4A2, is selectively upregulated in peripheral blood T cells from relapsing–remitting MS patients. Furthermore, using experimental autoimmune encephalomyelitis, an animal model of MS, we have shown that NR4A2 is selectively upregulated in peripheral blood T cells and T cells from inflamed CNS tissues. T cells expressing NR4A2 *in vivo* were induced only when immunized with self-peptide, not with irrelevant exogenous peptides. Accordingly, interleukin-17 (IL-17)-producing helper T cells exclusively express NR4A2, whether or not they secrete interferon (IFN)-γ, suggesting that NR4A2-expressing T cells represent a pathogenic Th17 subset during autoimmunity. Therefore, NR4A2 could be a useful biomarker to estimate pathogenic Th17 cell behavior in MS patients. In addition, a blockade of NR4A2 expression in differentiating Th17 cells with small interfering RNA not only abolished IL-17 secretion, but also Th17-related genes, such as IL-21, c-Maf and IL-23 receptor. Finally, *in vivo* administration of NR4A2-specific small interfering RNA significantly ameliorated experimental autoimmune encephalomyelitis, implying that NR4A2 is essential for triggering MS/experimental autoimmune encephalomyelitis, and could serve as a novel therapeutic target of the diseases. (Clin. Exp. Neuroimmunol. doi: 10.1111/cen3.12128, May 2014)

Introduction

Multiple sclerosis (MS) is a complex disease of the central nervous system (CNS) in which inflammatory and neurodegenerative processes cause intermittent neurological disorder and subsequent progression of debilitating symptoms. In general, MS is categorized into several major disease forms, including the most common form, relapsing–remitting MS (RR-MS), which sometimes exacerbates into secondary progressive MS (SP-MS), and the less frequent form primary progressive MS (PP-MS).[1] Although the etiology and specific causes of MS are not well understood, the susceptibility for individuals to develop MS could be attributed to both genetic (e.g. disease susceptibility genes) and environmental (e.g. external and internal environmental microorganisms) factors. Recent genome-wide association studies (GWAS) have identified many potential risk loci and multiple variants that might have a key role

in disease susceptibility.[2,3] Of note, these studies highlight a number of immunologically relevant genes, particularly those linked to helper T cell differentiation and function, suggesting the intrinsic participation of T cell components for MS pathogenesis.[4] As such, interest in interventions against autoreactive T cells to treat MS has grown, resulting in recently-developed therapies and ongoing clinical trials, such as those using natalizumab (humanized anti-α 4 integrin monoclonal antibody), fingolimod (FTY720) and glatiramer acetate, all of which are aimed to mitigate excessive immune responses of autoreactive T cells.

Organ-specific autoimmune diseases, including MS, emerge when autoreactive T cells primed in the periphery infiltrate into the CNS where reactivation of those T cells *in situ* initiates local damage and drives the recruitment of other inflammatory components (macrophages, B cells, granulocytes etc.). In early studies of MS, the major cause of organ-specific autoimmunity was believed to be the induction of immune responses by Th1 cells secreting interferon (IFN)-γ. However, recent studies have shown that autoimmune responses mediated by T helper 17 (Th17) cells secreting interleukin (IL)-17 might play key roles in the induction of autoimmune diseases. Accordingly, the role of Th17 cells in MS has been highlighted in recent years, and a large body of research has shown that such T cell responses could potentiate the pathogenesis of CNS-specific autoimmune inflammation; for example, elevated IL-17 responses and increased IL-17-secreting T cell numbers have been detected in MS patients, and correlate with active MS relapses.[5,6] Furthermore, Th17 responses have also been observed in the case of experimental autoimmune encephalomyelitis (EAE). Th17 responses appear to be critical for the induction of EAE as the severity of EAE was greatly reduced in mice lacking IL-23, IL-23R, IL-17 or IL-17R.[7–10] Interestingly, the CNS milieu in established EAE provides signals that preferentially drive Th17 responses.[11] As diverse sites, such as secondary lymphoid organs and peripheral circulation, as well as tertiary lymphoid-like structures, particularly those in the target organ (s), are involved in the development of organ-specific autoimmunity, the dynamics of the process by which pathogenic Th17 cells develop in EAE and MS have not yet been fully elucidated.

Through comprehensive gene expression profiling analysis, we previously showed that NR4A2, an orphan nuclear receptor that plays a versatile role in many aspects of biological and pathological responses, is selectively upregulated in the peripheral blood T cells of RR-MS patients in remission compared with healthy subjects.[12] Using EAE, an animal model of MS, we have further shown that NR4A2 is selectively upregulated in both T cells isolated from peripheral blood and those infiltrating into the CNS, but not from T cells in secondary lymphoid organs, such as the spleen and draining lymph nodes.[13,14] Here, the possible link between Th17 cells expressing NR4A2 and their pathogenic properties for CNS autoimmunity is summarized, the molecular mechanism of NR4A2-mediated Th17 cell differentiation is discussed, and the potential clinical application of NR4A2 as a novel therapeutic target for CNS autoimmunity with experimental data using small interfering RNA (siRNA) targeting the NR4A2 gene is suggested.

Th17 cells and EAE, an animal model of MS

Naive CD4+ T cells differentiate into Th1 cells on antigenic exposure in the presence of IL-12, and, once differentiated, Th1 cells maintain their phenotype even in different cytokine milieus, suggesting the relative robustness of the Th1 phenotype. In contrast, inflammatory processes crucial for Th17 differentiation are currently less understood. Originally, Th17 differentiation *in vitro* was observed after stimulation of naive T cells in the presence of transforming growth factor (TGF)-β in combination with IL-6.[15,16] However, IL-21 has also been reported to act as a differentiation factor by supporting the expansion of developing Th17 cells in an autocrine manner, and as an inducer of IL-23R expression on Th17 cells.[17] In that case, IL-23 could act as a critical factor for the stabilization and maturation of the phenotype of Th17 cells that express IL-23R on their cell surface.[18] In addition, a combination of different cytokines, such as IL-1β, IL-6 and IL-23, in the absence of TGF-β induces differentiation of IL-17-producing cells that apparently have an increased pathogenicity compared with conventional Th17 cells obtained by cultures with TGF-β and IL-6.[19] Therefore, it is not necessarily clear which differentiation pathway is critical for the physiological emergence of pathogenic T cells secreting IL-17 *in vivo*, and all of the factors described here could contribute to the differentiation of those cells to a greater or lesser extent.

It is well known that Th17 cells express the master transcriptional regulator retinoic acid-related orphan receptor γt (RORγt), and the deletion of the RORγt gene leads to impaired Th17 cell differentiation and reduces the severity of EAE development.[16] Pheno-